DMD Fast Forward. Published on February 25, 2019 as DOI: 10.1124/dmd.118.085035
This article has not been copyedited and formatted. The final version may differ from this version.

DMD # 085035

TITLE PAGE

Mechanistic Assessment of Extrahepatic Contributions to Glucuronidation of Integrase Strand Transfer Inhibitors

Authors:

Stephanie N. Liu[1], Jessica Bo Li Lu[1], Christy J.W. Watson[2], Philip Lazarus[2], Zeruesenay Desta[1], and Brandon T. Gufford[1]

[1]Division of Clinical Pharmacology, Department of Medicine, School of Medicine, Indiana University, Indianapolis, IN

[2]Department of Pharmaceutical Sciences, College of Pharmacy and Pharmaceutical Sciences, Washington State University, Spokane, WA

DMD # 085035

Running Title: Glucuronidation of Integrase Strand Transfer Inhibitors

Corresponding Author:

Zeruesenay Desta, PhD

Department of Medicine, Division of Clinical Pharmacology

Indiana University School of Medicine

950 W. Walnut Street, R2, Room 425

Indianapolis, IN 46202-5188

Phone: (317) 274-2823

Fax: (317) 278-2765

Email: zdesta@iu.edu

Word count:

Number of text pages: 43

Number of tables: 5

Number of figures: 6

Number of references: 47

Number of words in abstract: 247

Number of words in introduction: 719

Number of words in discussion: 1395

Abbreviations: HIV, human immunodeficiency virus; DDIs, drug-drug interactions; CYP, cytochrome P450; HEK293, human embryonic kidney 293; HLMs, human liver microsomes; HKMs, human kidney microsomes; HIMs, human intestinal microsomes; IVIVE, *in vitro in vivo* extrapolation; LC-MS/MS, liquid chromatography-tandem mass spectrometry; m/z, mass-to-charge ratio; PBPK, physiologically-based pharmacokinetic; rUGT, recombinant UGT; UDPGA, UDP-glucuronic acid; UGT, UDP-glucuronosyltransferase

Abstract

Integrase strand transfer inhibitor (INSTI)-based regimens dominate initial HIV treatment. Most INSTIs are metabolized predominantly via UDP-glucuronosyltransferases (UGTs). For drugs predominantly metabolized by UGTs, including INSTIs, *in vitro* data recovered from human hepatic microsomes (HLMs) alone often underpredict human oral clearance. While several factors may contribute, extrahepatic glucuronidation may contribute to this underprediction. Thus, we comprehensively characterized the kinetics for the glucuronidation of INSTIs (cabotegravir, dolutegravir, and raltegravir) using: pooled human microsomal preparations from liver (HLMs), intestinal (HIMs) and kidney (HKMs) tissues; HEK293 cells expressing individual UGTs; and recombinant UGTs (rUGTs). *In vitro* glucuronidation of cabotegravir (HLMs≈HKMs>>>HIMs), dolutegravir (HLMs>HIMs>>HKMs) and raltegravir (HLMs>HKMs>> HIMs) occurred in hepatic and extrahepatic tissues. The kinetic data from expression systems suggested the major enzymes in each tissue: hepatic UGT1A9>UGT1A1 (dolutegravir and raltegravir) and UGT1A1 (cabotegravir); intestinal UGT1A3>UGT1A8>UGT1A1 (dolutegravir) and UGT1A8>UGT1A1 (raltegravir); and kidney UGT1A9 (dolutegravir and raltegravir). Enzymes catalyzing cabotegravir glucuronidation in the kidney and intestine could not be identified unequivocally. Using data from dolutegravir glucuronidation as a prototype, a “bottom-up” physiologically based pharmacokinetic (PBPK) model was developed in a stepwise approach and predicted dolutegravir oral clearance within 4.5-fold (hepatic data only), 2-fold (hepatic and intestinal data), and 32% (hepatic, intestinal, and renal data). These results suggest clinically meaningful glucuronidation of dolutegravir in

tissues other than the liver. Incorporation of additional novel mechanistic and physiologic underpinnings of dolutegravir metabolism along with *in silico* approaches appear to be a powerful tool to accurately predict the clearance of dolutegravir from *in vitro* data.

Introduction

The human immunodeficiency virus (HIV) type 1 infection and the acquired immune deficiency syndrome *(*AIDS*)* is a global major public health problem. The prevalence of new HIV-1 infections and AIDS-related morbidity and mortality have considerably decreased over the past 35 years due in part to the continued development of new, highly effective HIV drugs that work by different mechanisms and introduction of novel formulations and drug combinations (Flexner 2019). HIV-1 infection has now evolved into a manageable disease that requires lifelong drug therapy. Thus, improving tolerability, efficacy and cost-effectiveness of these regimens in the context of a chronic care model has become an important consideration. However, over 35 million people still live with HIV/AIDS globally (over 1 million in the USA) and over 900,000 people died of HIV-related illnesses in 2017 alone (CDC, 2018; WHO 2019).

Due to their demonstrated clinical efficacy and excellent safety, integrase strand transfer inhibitors (INSTIs) in combination with two nucleos(t)ide reverse transcriptase currently dominate HIV therapy for both antiretroviral naïve- and experienced patients (HIV guidelines 2018). Four INSTIs (bictegravir, dolutegravir, raltegravir and elvitegravir) have been FDA approved and are recommended as preferred initial regimens for most treatment naïve HIV patients (HIV guidelines 2018; Flexner 2019). Cabotegravir is being developed as both an oral and long-acting injectable formulations (phase III drug development) for both the treatment and prevention of HIV infection (Flexner 2019). Glucuronidation via uridine diphosphate-glucuronosyltransferase (UGT) enzymes (e.g., hepatic UGT1A1) is the main metabolic pathways of dolutegravir, raltegravir and cabotegravir (Figure 1) (Kassahun et al., 2007; Castellino et al., 2013; Bowers et al.,

2016). Elvitegravir undergoes oxidation by cytochrome P450 (CYP) 3A (Mathias AA et al., 2009), and both oxidation (CYP3A) and glucuronidation are involved in the metabolism of bictegravir (Gilead Sciences, Inc., 2017).

UGTs are typically low affinity, high capacity enzyme systems that have minimal consequences on drug exposure from drug perpetrators (Gufford et al., 2015, Williams et al., 2004). Those INSTIs and other drugs mainly cleared by UGTs are thought to be less susceptible to drug-drug interactions (DDIs) than those observed with substrates of CYPs (Williams et al., 2004; Adams et al., 2012; Trezza et al., 2015; HIV guidelines 2018;). As a result, UGT mediated metabolism is an attractive property for new molecular entities undergoing development due to the confidence in stable metabolic elimination of the compound (Argikar et al., 2016). However, accurate *in vitro to in vivo* extrapolation (IVIVE) of clinical pharmacokinetics for drugs metabolized via UGT remains elusive (Argikar et al., 2016). Early phase development of the INSTIs found *in vitro* and preclinical data reported underprediction of apparent oral clearance (Laufer et al., 2009). This tendency is observed across several UGT substrates from other therapeutic classes (Boase and Miners, 2002; Soars et al. 2002; Laufer et al., 2009). This underprediction may be due to inadequate applications of the mechanistic and physiologic characteristics of the glucuronidation pathway and an inadequate understanding of the contribution of UGTs other than hepatic UGT1A1 (Izukawa et al., 2009; Court et al., 2012; Achour et al., 2017). Multiple UGTs, including UGT1A1, are expressed in multiple tissues at varying drug metabolizing capacity such as the liver, kidney, and intestine (Court el al., 2012, Drodzik et al., 2017, Gill et al., 2013, Margaillan et al., 2015). The possibility that UGTs in extra-hepatic tissues may catalyze the metabolism of INSTIs has not been previously

investigated. Further, the contribution of extrahepatic glucuronidation to overall systemic clearance of INSTIs remains unknown. The impact of factors (e.g., DDIs, organ function and genetic variations) influence the exposure via modulation of extrahepatic UGTs remains elusive. Developing accurate prediction framework of *in vivo* clearance from *in vitro* data of INSTIs and other UGT substrates accounting for extrahepatic metabolism is an important step to understand mechanisms influencing systemic exposure and effect of INSTIs.

The primary objective of this work was to apply an integrative approach that incorporated extrahepatic glucuronidation with our current understanding of hepatic INSTIs glucuronidation to improve understanding of clearance mechanisms and predictions of *in vivo* pharmacokinetics from *in vitro* data of INSTIs. Thus, *in vitro* enzyme kinetic parameters were recovered to quantitatively describe the major tissue-, isoform-, and pathway- specific UGT -mediated metabolism of cabotegravir, dolutegravir, and raltegravir. Using dolutegravir as an example, the *in vitro* hepatic and extrahepatic glucuronidation parameters were then incorporated into a PBPK model to predict clinical pharmacokinetics.

Materials and Methods

Materials and Chemicals.

Pooled human liver microsomes (HLMs) from 50 donors with mixed sex [average age: 47 years old (range, 5-83)], pooled human kidney microsomes (HKMs) from 8 donors with mixed sex [average age: 54 years old (range, 42-70)] and pooled human intestinal microsomes (HIMs) from 15 donors with mixed sex [average age: 54 years old (range, 26-69)] were purchased from Xenotech, LLC (Lenexa, KS). UDP-glucuronosyltransferase (UGT) expressing baculovirus-insect cell systems (Supersomes™) were purchased from Corning Incorporated (Woburn, MA). Human embryonic kidney (HEK293) cells overexpressing individual UGT1A enzymes were harvested, and microsomes prepared as described previously (Sun et al., 2013). Cabotegravir and dolutegravir and were purchased from MedChemExpress, LLC (Monmouth Junction, NJ). Raltegravir was obtained from NIH AIDS Reagent Program (Germantown, MD). Cabotegravir glucuronide, dolutegravir glucuronide, and raltegravir glucuronide were purchased from Toronto Research Chemicals Inc. (North York, Canada) and were 95% pure as determined by the supplier via thin layer chromatography with nuclear magnetic resonance spectroscopy and mass spectrometry structural confirmation. Alamethicin, magnesium chloride, 8-14-dihydroxy efavirenz, nevirapine, saccharolactone, Tris-HCl, Tris base, and UDP-glucuronic acid (UDPGA) were purchased from Sigma (St Louis, MO). Dimethylsulfoxide, acetonitrile (ACN), methanol, ethanol, and formic acid (all liquid chromatography-mass spectrometry grade) were purchased from Fisher Scientific (Hampton, NH). Dialysis membranes (12-14 kDa molecular mass cutoff) were purchased

from Fisher Scientific (Hampton, NH). The 96-well micro-equilibrium HTD 96b dialysis device was obtained from HTDialysis, LLC (Gales Ferry, CT).

LC-MS/MS Method Development

A new LC-MS/MS method was developed for quantification of cabotegravir, dolutegravir, raltegravir, and their respective glucuronide metabolites. Chromatographic separation was accomplished using a Phenomenex Luna C18, 5µM, 4.6x150 mm column (Torrance, CA) heated to 30°C with a binary gradient flow of 0.8 mL/min. The gradient elution began with 40:60 acetonitrile:water (both with 0.1% formic acid) and increased to 90:10 at 5 minutes and held for 0.5 minutes before returning to initial conditions for the remaining 2 minutes. Chromatographic separation was achieved within 7.5 minutes using a single LC method for all compounds (Supplemental Figure 1). Samples were analyzed (3µL injection volume) using the QTRAP 6500+ LC-MS/MS system (AB Sciex, Framingham, MA) with turboelectrospray source operated in both positive (confirmation) and negative (quantification) mode. The negative mode was used to improve glucuronide metabolite sensitivity and selectivity with confirmatory transitions in positive ion mode. 8-14-dihydroxy efavirenz and nevirapine were used as internal standards for the negative and positive mode, respectively. Compound specific instrument parameters were optimized for each analyte (Supplemental Table 1). The incubation-generated INSTI glucuronides were directly quantified using commercially available INSTI glucuronide authentic standards with a dynamic assay range of 0-2000 nM. The instrument response was linear with respect to increasing analyte concentration over the standard curve range used. The lower limit of quantification (LLOQ) was 1 nM (cabotegravir glucuronide) or 2

nM (dolutegravir and raltegravir glucuronides). Data were acquired using Analyst software (v. 1.6.3; AB Sciex) and quantified via MultiQuant software (v. 3.0.2; AB Sciex). Assay accuracy was evaluated using MultiQuant software; standard and quality control samples were deemed acceptable if within 20% of nominal value except for the LLOQ that was assessed with a 30% threshold.

Glucuronidation Kinetics in HLMs, HIMs and HKMs

Incubation conditions were optimized for each substrate and enzyme source to ensure linearity of metabolite formation with respect to time and protein concentration and to prevent greater than 20% substrate depletion (Supplemental Table 2). To determine the kinetics for the formation of the glucuronides, cabotegravir, dolutegravir, and raltegravir (concentrations spanning 0-2000 µM) were incubated in duplicate with each individual tissue microsomal preparations (HLMs, HIMs and HKMs protein concentrations shown in Supplemental Table 2) in Tris HCL buffer (pH 7.4, 100 mM) containing $MgCl_2$ (5 mM) and bovine serum albumin (BSA) (0.05%) with a total incubation volume of 150 µL. HLMs, HIMs, and HKMs were treated with alamethicin (50 µg/mg protein) on ice for 15 minutes. Saccharolactone (100µM) was added to all HIMs preparations. Mixtures were equilibrated at 37°C for 5 minutes and reaction was initiated by the addition of 15 µL UDPGA (2 mM final concentration) and incubated for 60 (cabotegravir), 30 (dolutegravir), and 20 (raltegravir) minutes. Reactions were terminated by removing 100 µL from the incubation and diluting into 300 µL ice-cold acetonitrile (0.1% formic acid) containing internal standards nevirapine (0.2 µM) and 8,14-dihydroxy efavirenz (0.2 µM). Samples

DMD Fast Forward. Published on February 25, 2019 as DOI: 10.1124/dmd.118.085035
This article has not been copyedited and formatted. The final version may differ from this version.

were vortex-mixed and centrifuged at 3000 x g for 20 minutes at 4°C. Supernatant (200 µL) was transferred to clean 96-well plates for analysis via LC-MS/MS.

Determination of Non-Specific Protein Binding in HLMs, HIMs, and HKMs

The equilibrium dialysis method described by Gill et al., 2012 was used to determine fraction unbound in the incubation, $f_{u,inc}$, values for all three drugs (cabotegravir, dolutegravir, raltegravir) in pooled HLMs, HIMs, and HKMs in the presence and absence of BSA. Each INSTI drug (10 µM) in buffer was added to the donor side of the membr along the relevant concentration of microsomal protein (Supplemental Table 2) with or without BSA (0.05%). Tris-HCl buffer (pH 7.4, 100 mM) containing $MgCl_2$ (5 mM), and saccharolactone (100 µM) (for HIMs only), was added to the acceptor side of the membrane. Experiments were performed in duplicate. The plate was left to equilibrate for 6 h on a plate shaker (250 rpm) at 37°C. Aliquots (50 µL) were transferred from both the acceptor and donor side of the membrane to 200 µL containing the internal standard nevirapine (0.2 µM) and methanol (0.1% formic acid). Samples were vortex-mixed and centrifuged at 3000 rpm for 20 min at 4°C. Supernatant (100 µL) was transferred to clean 96-well plates for analysis via LC-MS/MS as described above. Fraction unbound was calculated as follows:

$$f_{u,inc} = \frac{(\text{peak area in acceptor side } (+\text{BSA}))/(peak\ area\ internal\ standard\ (+BSA)\ )}{(\text{peak area in donor side } (-\text{BSA}))/(peak\ area\ internal\ standard\ (-BSA)\ )}$$

Reaction Phenotyping using a Recombinant UGT Enzyme Panel

Cabotegravir, dolutegravir, or raltegravir (50 µM) were incubated in duplicate with each individual rUGT enzyme (0.2 mg/mL rUGT 1A1, 1A3, 1A4, 1A6, 1A7, 1A8, 1A9,

1A10, 2B4, 2B7, 2B15, 2B17) or vehicle/vector control as described above except for the absence of alamethicin and saccharolactone. Reactions were initiated by the addition of 15 µL UDPGA (2 mM final concentration) and terminated at 60 minutes by transferring 100 µL of each incubation into 300 µL of ice-cold acetonitrile (0.1 % formic acid) containing internal standard and analyzed via LC-MS/MS as described above.

Isoform Specific Glucuronidation Kinetics

Ranging concentrations of cabotegravir, dolutegravir, or raltegravir (0-2000µM) were incubated in duplicate with each UGT enzyme source: rUGT1A1, rUGT1A3, rUGT1A7, rUGT1A8, rUGT1A9, HEKUGT1A1, HEKUGT1A3 (raltegravir only), HEKUGT1A7, HEKUGT1A8, HEKUGT1A9 using isoform-specific optimized conditions for protein concentration and incubation time (Supplemental Table 2). Incubation vehicle/vector and reaction initiation mirrored that described for the microsomal preparations except for the absence of alamethicin in rUGT preparations. The rUGT and HEKUGT incubations did not use saccharolactone. All rUGT incubations were completed using a single manufacturer lot.

Physiologically Based Pharmacokinetic Model Development

Dolutegravir was selected as a prototype for further evaluation of the *in vivo* contributions of extrahepatic tissues in INSTIs metabolism via physiologically based pharmacokinetic (PBPK) modeling using SimCYP (v. 16.0). Modeling dolutegravir was selected in this manuscript for a number of reasons: 1) it is the most commonly prescribed clinically; 2) it has sufficient clinical data readily available to confirm model predictions;

and 3) published PBPK models are lacking. The PBPK model was parameterized initially using literature values to describe dolutegravir physicochemical properties and oxidative metabolism (Supplemental Table 3) (Castellino et al., 2013, Reese et al., 2013). The ADAM model was selected for incorporation of intestinal glucuronidation and dynamic multi-compartmental transit time effects. Standard SimCYP model parameters of potential enterohepatic circulation (100%) from the compound eliminated from biliary excretion was incorporated. Glucuronidation kinetics were described in a step-wise fashion via incorporation of *in vitro* enzyme kinetic parameters describing hepatic only, hepatic plus renal, and finally the combination of hepatic, renal, and intestinal UGT-mediated metabolism. Simulations were conducted using the SimCYP 'healthy volunteers' multiple populations [10 trials with 10 subjects (20-50 years old) in each trial] administered a single 50 mg oral dolutegravir dose. Published dolutegravir clinical pharmacokinetic data with a matching dosing regimen (single fasted 50 mg dose in healthy volunteers) (ViiV Healthcare, 2013; Song et al., 2015) was used in the evaluation of PBPK model predictions and recovered using GetData® Graph Digitizer (v. 2.26.0.20). Sensitivity analyses were conducted to quantitatively assess the impact of extrahepatic glucurdonidation parameter (HIMs and HKMs Cl_{int} values) uncertainty on the pharmacokinetic outcomes of interest (C_{max}, AUC, and Cl_{PO}) (Supplemental Figure 2).

Data Analyses

Apparent kinetic constants for glucuronidation of the test substrates were obtained via nonlinear regression by fitting Michaelis–Menten, substrate inhibition, two site, or Hill

DMD Fast Forward. Published on February 25, 2019 as DOI: 10.1124/dmd.118.085035
This article has not been copyedited and formatted. The final version may differ from this version.

equations to substrate concentration ([S]) versus apparent metabolite formation velocity data using Phoenix® WinNonlin® (v. 7.0).

The Michaelis−Menten equation is as follows: $= \frac{V_{max}*[S]}{K_m+[S]}$, where *v* is the initial rate of reaction, V_{max} is the maximum velocity, K_m is the Michaelis−Menten constant (substrate concentration at 0.5 V_{max}), and [S] is the substrate concentration.

Hill equation: $= \frac{V_{max}*[S]^n}{S_{50}^n+[S]^n}$, where S_{50} is the substrate concentration resulting in 50% of V_{max} (analogous to K_m in the previous equation) and *n* is the Hill coefficient.

Two site: $v = \frac{V_{max1}*[S]}{K_{m1}+[S]} + \frac{V_{max2}*[S]}{K_{m2}+[S\}}$, where V_{max1}, V_{max2} are the maximum velocities and K_{m1}, K_{m2} are the Michaelis−Menten constants for the two sites of the enzyme.

Substrate inhibition: $v = \frac{V_{max}*[S]}{K_m+[S]*(1+\frac{[S]}{K_i})}$, where K_i is the inhibition constant.

K_m and S_{50} were corrected for non-specific binding $K_m * f_{u,inc}$ ($K_{m,u}$ and $S_{50,u}$). *In vitro* $Cl_{int,u}$ ($V_{max}/K_{m,u}$) or $Cl_{max,u}$ (V_{max} x (h-1)/$K_{m,u}$ + h(h-1)$^{1/h}$) (Houston and Kenworthy, 2000), where *in vitro* $Cl_{int,u}$ is the unbound intrinsic clearance per microsomal protein and calculated for substrates described by the simple Michaelis−Menten or Hill equation, respectively. Best-fit models were selected by visual inspection of the predicted versus observed data, precision of parameter estimates generated from the nonlinear regression, and Akaike information criteria. Unless noted, data are presented as mean of duplicate incubations, with error bars showing data variability for *N* = 2.

Scaling from *in vitro* Cl_{int} to organ Cl_{int}

The *in vitro* $Cl_{int,u}$ was used to estimate whole organ Cl_{int}*: as follows: in vitro* $Cl_{int,u}$ * *scaling factor (MPPGL, MPPGK, or MPPI) * organ weight (liver or kidney)*, where

MPPGL is the microsomal protein per gram of liver, MPPGK is the microsomal protein per gram of kidney, and MPPI is the microsomal protein per total intestine. The following scaling factors were used: MPPGL of 37.69 mg mics / g of liver tissue (Wood et al. 2017) (total liver wieight = 1800 g)(Davies and Morris 1993); MPPGK of 12.8 mg mics / g of renal tissue (Al-Jahdari et al. 2006) (total kidney weight = 310 g) (Davies and Morris 1993); and MPPI 2935.17 mg mics / total intestine (Paine et al. 1997). The microsomal scaling factors are imbedded in SimCYP software.

Results

INSTIs Glucuronidation is Tissue Dependent

Glucuronidation kinetic parameters were recovered with varying concentrations (0-2000µM) of cabotegravir, dolutegravir, and raltegravir in pooled HLMs, HKMs, and HIMs to quantitatively assess tissue-specific INSTI glucuronidation (Figure 2 and Table 1). To correct the K_m values derived for nonspecific protein binding in incubation ($f_{u,inc}$), equilibrium dialysis experiments were performed in pooled HLMs, HIMs and HKMs. Incubations tested in the absence of albumin found $f_{u,inc}$ was ≥0.85 for cabotegravir, dolutegravir, and raltegravir. Nonspecific protein binding was observed in the presence of BSA for dolutegravir and cabotegravir, while the fraction unbound for raltegravir was unaffected by either BSA or microsomal proteins ($f_{u,inc}$ was ≥0.90) (Table 1). Pooled HLMs had the greatest nonspecific protein binding for dolutegravir and HKMs for cabotegravir. There were minimal differences in protein binding between the different organ tissues (HLMs, HIMs, HKMs) for the same substrate but noticeable changes in binding among the different INSTI substrates (Table 1). The fraction unbound ($f_{u,inc}$) was then used to estimate the unbound K_m ($K_{m,u}$) values (Table 1) and accordingly, the *in vitro* $Cl_{int,u}$ was calculated (Table 1). In the subsequent portion of the manuscript, K_m is referred to $K_{m,u}$ and *in vitro* intrinsic clearance (Cl_{int} is $Cl_{int,u}$).

Cabotegravir and raltegravir appeared to be relatively low affinity substrates for UGTs as represented by high K_m values (167-560 µM) (Table 1), while the K_m values for dolutegravir was between 32-96 µM. Microsomal UGTs had the lowest affinity for cabotegravir in all three tissues compared to dolutegravir and raltegravir, suggesting slower metabolism via UGT for cabotegravir. Cabotegravir glucuronide was most efficiently (*in vitro* Cl_{int}) formed in HLMs and HKMs compared to HIMs. The K_m values

DMD Fast Forward. Published on February 25, 2019 as DOI: 10.1124/dmd.118.085035
This article has not been copyedited and formatted. The final version may differ from this version.

for cabotegravir glucuronidation was relatively high and saturation was not easily achieved in the case of HIMs, suggesting that this elimination pathway is low affinity and high capacity, a common observation for UGT-mediated elimination routes. Thus, K_m (>6 mM) and V_{max} values were unreliable to estimate *in vitro* Cl_{int}.

Overall, the *in vitro* metabolism of cabotegravir in HIMs was relatively small, suggesting minimal intestinal contribution to the overall metabolic clearance. Intestinal UGT's expressed the lowest affinity (highest K_m) and highest capacity (V_{max}) for dolutegravir, while HLMs and HKMs showed relatively lower K_m values (Table 1). Based on the *in vitro* Cl_{int}, dolutegravir glucuronidation was more efficient in HLMs (1.5- and 3-fold higher compared to HIMs and HKMs, respectively). The microsomal preparations suggested raltegravir glucuronidation was more similar to cabotegravir in terms of tissue involvement. Raltegravir was glucuronidated predominantly in HLMs and HKMs with lesser HIMs contributions. Raltegravir glucuronidation was higher in hepatic tissue, reflected by the 4.8-fold greater Cl_{int} compared to intestinal tissue and 2-fold greater compared to renal tissues. Renal tissue expressed the lowest affinity (K_m), but the highest UGT capacity (V_{max}) for raltegravir.

The *in vitro* $Cl_{int,}$ was used to estimate *in vivo* organ Cl_{int}. In contrast to the *in vitro* data showing clear contributions of extrahepatic glucuronidation, the *in vivo* Cl_{int} data predicted from the *in vitro* kinetic parameters indicate predominant role of hepatic metabolism of these drugs (Table 1).

INSTIs Glucuronidation in Recombinant UGTs

Microsomal enzyme kinetic data revealed the prominent role of extrahepatic INSTI glucuronidation and formed the basis for further evaluation of isoform-specific INSTI

DMD Fast Forward. Published on February 25, 2019 as DOI: 10.1124/dmd.118.085035
This article has not been copyedited and formatted. The final version may differ from this version.

glucuronidation. Reaction phenotyping was conducted using recombinant UGT expressing baculovirus-insect cell systems to qualitatively identify specific UGT enzymes responsible for formation of the respective INSTI glucuronides (Figure 3). The reaction phenotyping showed that rUGT1A9 and rUGT1A1 catalyzed glucuronidation of cabotegravir, dolutegravir, and raltegravir at the highest rate. Other isoforms also participate to a small extent in the glucuronidation of cabotegravir (rUGT1A3 << rUGT1A7 < rUGT1A8), dolutegravir (UGT1A3 ≈ UGT1A8), and raltegravir (UGT1A7 < UGT1A8 < UGT1A3).

For those isoforms that showed activity (UGT1A1, UGT1A3, UGT1A7, UGT1A8 and UGT1A9), UGT isoform-specific INSTI glucuronidation was evaluated in more detail by recovering UGT enzyme-specific glucuronidation kinetic parameters. Representative substrate concentration versus velocity curves of UGT1A9 and UGT1A1 fit to Michaelis-Menten or Hill are equation shown in Figure 4. All three INSTIs exhibited substrate inhibition kinetics in rUGT1A9 at concentrations above 1000 μM. Since these concentrations are supratherapeutic they were removed to simplify the kinetics to fit the Hill equation. Kinetic parameters derived for all rUGTs tested are listed in Table 2. Since the determining factor influencing nonspecific binding was BSA, which was common for incubations with HLMs and the expression systems, $f_{u,inc}$ was not estimated for each UGT isoform. Instead, $f_{u,inc}$ derived from HLMs (see above) was used to account for nonspecific binding to correct the K_m values derived from the expression systems. Accordingly, adjusted K_m ($K_{m,u}$) and Cl_{int} ($Cl_{int,u}$) values are calculated and presented for each enzyme (Table 2). Because information on the specific UGT protein content was not available or provided from the supplier, the V_{max} and Cl_{int} should be viewed as nominal values. To

DMD Fast Forward. Published on February 25, 2019 as DOI: 10.1124/dmd.118.085035
This article has not been copyedited and formatted. The final version may differ from this version.

obtain insight into tissue-specific metabolism, the K_m values derived from these isoforms (Table 2) are compared with those obtained from HLMs, HIMs and HKMs (Table 1). The K_m values for the formation of cabotegravir glucuronide was much higher in both HIMs and HKMs (Table 1) than any of those derived from the rUGTs (Table 2). Only the K_m value of rUGT1A8 was close to that in HLMs, but, given that UGT1A8 is mainly expressed in the gut-wall, this relationship cannot be fully explained. The K_m for UGT1A9-mediated cabotegravir glucuronidation was more than 6-fold lower than in HLMs. K_m values derived from rUGTs (rUGT1A3, 1A8 and 1A9) were close to those for dolutegravir glucuronidation in HLMs, HIMs and HKMs. Of note, the K_m value for dolutegravir glucuronidation in rUGT1A1 was much higher (216 μM). Finally, the K_m values for the formation of raltegravir glucuronide in HLMs and HIMs were close to those derived from rUGT1A1 and rUGT1A9.

INSTIs Glucuronidation Kinetics in HEK cells expressing individual UGTs

Full UGT isoform-specific INSTI glucuronidation kinetics were further evaluated using selected HEK cells expressing individual UGTs (Table 3). A majority of the substrate concentration versus velocity curves fit the Michaelis-Menten equation but some fit to atypical non-hyperbolic enzyme kinetics and were better described by the sigmoidal equation (Hill equation). The substrate concentration versus velocity curves for the glucuronidation of the INSTIs by UGT1A1 and UGT1A9 expressed in the HEK293 cell system are shown in Figure 5, with the corresponding kinetic parameters derived for all UGTs shown in Table 3. As with rUGTs, isoform-specific protein expression was not available in the sub-cellular fraction of the cell lines. Therefore, V_{max}

DMD Fast Forward. Published on February 25, 2019 as DOI: 10.1124/dmd.118.085035
This article has not been copyedited and formatted. The final version may differ from this version.

and Cl_{int} presented (Table 3) are only adjusted for total protein amount and should be viewed as nominal or relative values and should not be quantitatively compared between and within cell systems (rUGTs and HEK UGTs). The K_m values for cabotegravir glucuronidation in HEK cells (1A1 = 55 µM and 1A9 = 163 µM) were higher than those in rUGT1A1 and rUGT1A9 and were closer to the K_m value in hepatic (HLMs) (350 µM), although the values are still notably lower (by approximately 3-6-fold) than observed in HLMs. The K_m value in intestinal tissue (in mM range) for cabotegravir do not concur with any of the K_m values derived from HEK cell UGT isoforms. The reason for this discrepancy is not clear. The K_m values for dolutegravir glucuronidation in HEK cells (1A9 = 46 µM) is close to the K_m value obtained from HLMs (32µM) and HKMs (K_m = 47µM); the K_m value for the other hepatic UGT examined in HEKs (1A1 = 96 µM) was 3-fold higher than in HLMs. Thus, UGT1A9 (and to a lesser extent 1A1) appears to be the main enzymes responsible for dolutegravir glucuronidation in the liver and kidney. Dolutegravir glucuronidation in HIMs (K_m = 96 µM) appears to concur with UGT1A1 and UGT1A8 (HEK cell UGT1A1 = K_m = 96 µM; UGT1A8 K_m = 37 µM). The K_m value for raltegravir glucuronidation in UGT1A9 expressed in HEK cells (K_m = 219 µM) was closer to that derived from HLMs (K_m = 183 µM). The K_m values derived from this enzyme (HEKUGT1A9) were about half of that observed for raltegravir glucuronidation in HKMs. This enzyme may in part explain hepatic and renal glucuronidation of raltegravir. Considering the lower K_m value by UGT1A1 expressed in HEK cells and comparable K_m in rUGT1A1 to that in HLMs, it seems that both UGT1A1 and UGT1A9 are the active UGTs in raltegravir glucuronidation. UGT1A8 appears important for

raltegravir glucuronidation in the gut-wall (K_m value in UGT1A8 expressed in HEK cells = 142 µM versus 167 µM in HIMs).

Extrahepatic Glucuronidation Contributes to INSTIs Metabolism

Dolutegravir *in vitro* glucuronidation kinetics from microsomal data were incorporated into a physiologically-based pharmacokinetic model using SimCYP® to predict dolutegravir clinical pharmacokinetics. After recovering substantial dolutegravir glucuronidation in intestinal tissue, the ADAM absorption model was selected to input the intestinal glucuronidation parameters recovered in HIMs. Three PBPK models were generated to predict dolutegravir clinical pharmacokinetics: 1) *in vitro* hepatic glucuronidation clearance only 2) *in vitro* hepatic and intestinal glucuronidation clearance 3) *in vitro* hepatic, intestinal, and renal glucuronidation clearance (Figure 6). Empiric scaling factors were applied to the intestinal and renal glucuronidation intrinsic clearance (Cl_{int}) parameters as these could not be input via the more mechanistic approach using the UGT isoform and tissue specific K_m and V_{max} parameters. Sensitivity analyses of these extrahepatic glucuronidation parameters revealed that model predicted C_{max} and Cl_{PO} were more sensitive to changes in intestinal Cl_{int} while AUC was more sensitive to HKMs Cl_{int} (Supplemental Figure 1). All three models incorporated published values describing minor dolutegravir *in vitro* oxidative metabolism (CYP3A4) (Reese et al., 2013) and renal clearance. PBPK models underpredicted observed dolutegravir apparent oral clearance by 4.5-fold, 2-fold, or 32% by incorporating hepatic only, hepatic and intestinal, or hepatic, intestinal, and renal glucuronidation, respectively. The model incorporating glucuronidation in all three tissues predicted observed dolutegravir C_{max} and AUC_{0-24} within 18% and 38%, respectively (Table 4).

DMD Fast Forward. Published on February 25, 2019 as DOI: 10.1124/dmd.118.085035
This article has not been copyedited and formatted. The final version may differ from this version.

Discussion

This work is the first comprehensive *in vitro* characterization of cabotegravir, dolutegravir, and raltegravir glucuronidation in microsomes derived from liver and extrahepatic tissues, HEK293 cells expressing individual UGTs, and recombinant UGTs. We confirmed involvement of previously reported UGT isoforms and identified additional enzymes catalyzing the glucuronidation of these INSTIs. We report for the first time that these three INSTIs undergo substantial extrahepatic glucuronidation. Using dolutegravir *in vitro* hepatic and extrahepatic metabolism, we showed that a "bottom-up" PBPK model incorporating extrahepatic glucuronidation accurately predicted dolutegravir clinical pharmacokinetics from *in vitro* data. These results suggest the occurrence of clinically meaningful glucuronidation in tissues other than the liver, specifically intestine and kidney. Incorporation of additional novel mechanistic and physiologic underpinnings of dolutegravir metabolism along with *in silico* approaches appear to be powerful tools to accurately predict the clearance of dolutegravir from *in vitro* data.

Our data showed that all the INSTIs tested undergo efficient glucuronidation in HLMs. The INSTI hepatic UGT enzyme kinetic parameters reported in this work were similar to those values published in the literature (Kassahun et al., 2007, Reese et al., 2013, Trezza et al., 2015). Under prediction of oral clearance for UGT substrates using IVIVE approaches is quite common and several factors may contribute to this problem (Boase S and Miners, 2002, Soars et al., 2002). It is well established that UGTs are differentially expressed in hepatic and extrahepatic tissues (Guillemette et al., 2014; Margaillan et al., 2015; Drozdzik et al., 2017). Therefore, it is possible that this tissue-specific expression contributes to INSTI glucuronidation. Indeed, our data demonstrate

for the first time that these drugs undergo efficient extrahepatic glucuronidation in microsomes derived from human kidney and intestinal tissues. Based on the *in vitro* Cl_{int} displayed in Table 1: a) HLMs and HKMs equally contribute towards cabotegravir glucuronidation, with minor involvement of HIMs; b) HLMs then HIMs contributed to dolutegravir glucuronidation, with minor participation from HKMs; and c) the metabolism of raltegravir was approximately 2- and 5-fold higher in HLMs than in HKMs and HIMs, respectively. On the basis of *in vivo* Cl_{int}, we noted that HLMs alone provide a larger contribution to INSTIs glucuronidation with minor contribution from extrahepatic tissue in contrast to the data derived from *in vitro*. While understanding the total activity per organ is desirable, the uncertainty of absolute UGT amount in the gut and kidney makes this comparison less accurate. In addition, the *in vitro* data are only showing the ability of the enzyme systems in those tissues to metabolize the drugs. The *in vitro* data suggest that the gut and kidney are clearly capable of metabolizing the drugs. However, when considering factors such as the overall size of the organ, blood flow, drug uptakes and other physiological parameters, it is clear that the liver still plays a major role. There is no doubt that the liver is the main contributor but without including the gut and kidney, it is not possible to predict the pharmacokinetic behavior of these compounds accurately as shown in our dolutegravir PBPK model.

We tested the hypothesis that extrahepatic metabolism contributes to INSTIs glucuronidation *in vivo*. Using dolutegravir glucuronidation data derived from HLMs, HIMs and HKMs, we developed a PBPK model to show that incorporation of extrahepatic glucuronidation substantially improve the accuracy of PBPK model predictions (Figure 6). Although the absolute bioavailability of dolutegravir remains unknown, the high gut and

liver involvement in dolutegravir glucuronidation is suggestive of significant first pass metabolism, while kidney glucuronidation also contributes to systemic clearance (Supplemental Figure 2). This PBPK model will be tested and validated in the future for IVIVE for other INSTIs and substrates of UGTs.

The comprehensive characterization of the INSTIs glucuronidation in recombinant UGTs (Table 2) and in HEK293 cells expressing individual UGTs (Table 3) provide important insights into isoform-specific metabolism of these drugs as summarized in Table 5. We are aware that additional inhibition analysis could have added valuable information in addition to the K_m determinations. However, there are no selective and specific inhibitors of UGT that allow unequivocal identification of individual isoforms. Our data from expressed UGTs generally agree well with published literature identifying the enzymes active in the respective INSTI glucuronidation, however, qualitative differences are noted. We found that UGT1A9 and UGT1A1 are major contributors of cabotegravir, dolutegravir, and raltegravir metabolism, with contribution from other isoforms (UGT1A3, UGT1A7, and UGT1A8). Poor predictions were observed for cabotegravir metabolism in regards to the tissue-specific relationship to specific UGT isoforms due to large differences in K_m values. The supraphysiological K_m values in hepatic and extrahepatic tissues along with two-site enzyme kinetics (Figure 4) suggest multiple isoforms may be responsible for cabotegravir's glucuronidation in the different tissues. For dolutegravir, UGT1A9 K_m values were similar to that found in hepatic and renal tissue. Similarly, UGT1A1 and UGT1A9 K_m values were similar to hepatic and intestinal tissue with regard to raltegravir glucuronidation. This suggests UGT1A9 may be the major isoform responsible for hepatic glucuronidation of dolutegravir and

raltegravir. Considering that UGT1A9 is predominantly expressed in the kidney, this enzyme may also be the major isoform for renal glucuronidation of dolutegravir and raltegravir. UGT1A9 has been reported undetectable in gastrointestinal tissue (Strassburg et al., 2000; Komura H and Iwaki M 2011) and thus unlikely to contribute to the intestinal glucuronidation of raltegravir (and dolutegravir) despite similar K_m values in HIMs and UGT1A9 (Strassburg et al., 2000; Komura H and Iwaki M 2011). UGT1A1 appears to participate in hepatic and intestinal glucuronidation of raltegravir. Based on the K_m values in HEK cell expression system data, UGT1A8, an enzyme mainly expressed in the intestine (Strassburg et al., 2000; Komura H and Iwaki M 2011), appears to be important in the intestinal glucuronidation of dolutegravir and raltegravir. It is important to note that the kinetic data obtained from baculovirus-insect Supersomes® (rUGT) and HEK293 UGT overexpressed cell lysates should be interpreted carefully because they were normalized to total protein instead of specific UGT protein amount (Table 2 and 3). The K_m values between cell systems for the same isoform broadly agree with each other, with slight differences. It appears that HEK-expressed UGT1A8 and UGT1A9 correlate better with HIMs and HLMs, for dolutegravir and raltegravir glucuronidation. This additional layer of understanding may facilitate quantitative assessment of genetic variation and non-genetic perturbations to UGT metabolism caused by changes in the underlying system and may allow for better prediction of clinical impact.

The clinical relevance of pharmacogenomic variation contributing to the observed variability of integrase inhibitor disposition is limited for UGT1A1 and nearly nonexistent for UGT1A9 and the other UGTs. The *UGT1A1* gene is highly polymorphic, with common

genetic variants that reduce hepatic UGT1A1 activity (*6, *28, *36 and *37 are the most studied) (Yagura et al., 2015, Wenning et al., 2009, Adams et al., 2012). Chen et al., reported that dolutegravir clearance was significantly reduced and its exposure increased in carriers of low and reduced activity polymorphisms compared with subjects with normal activity (Chen et al., 2014). A similar statement is stated in the FDA approved dolutegravir package insert. A recent study showed that UGT1A1*6 and *28 alleles individually and in combination are significantly associated with higher dolutegravir plasma trough concentrations and neuropsychiatric events (Yagura et al., 2017). A similar response was seen with raltegravir (Wenning et al., 2009, Yagura et al., 2015, Belkhir et al., 2018, Lee et al., 2016). There is still much to learn about the clinical implications of genetic variability in the UGT system and the importance in patient response or safety. First, no data is available regarding pharmacogenetics of cabotegravir and the impact of genetic variations in other UGTs on INSTIs exposure remains unstudied. Second, the tissue-specific impact of pharmacogenomic variability in extrahepatic UGT expression and implications for drug metabolism remains relatively unexplored.

In summary, significant glucuronidation occurs in various tissues throughout the body with the liver, kidney, and intestine being particularly important for orally administered drugs. The degree of contribution from each tissue is UGT substrate- and isoform- specific and must be taken into account to improve *in vitro* prediction of *in vivo* behavior. Incorporation of *in vitro* hepatic, intestinal, and renal glucuronidation in a PBPK model achieved predicted dolutegravir clearance within 32%, C_{max} within 17%, and AUC_{0-24} within 38% of observed data. Dynamic modeling and simulation approaches, along with

clinical assessment, are needed to produce a useful tool to predict pertubations to the underlying system and individualize patient care.

Author Contributions

Participated in research design: SNL, JBL, ZD, BTG

Conducted experiments: SNL, JBL, CJWW, BTG

Contributed new reagents or analytical tools: BTG, JBL, CJWW, PL

Performed data analysis: SNL, BTG, ZD

Wrote or contributed to writing of the manuscript: SNL, JBL, CJWW, PL, ZD, BTG

References

Achour B, Dantonio A, Niosi M, Novak JJ, Fallon JK, Barber J, Smith PC, Rostami-Hodjegan A, Goosen TC (2017) Quantitative characterization of major hepatic UDP-glucuronosyltransferase enzymes in human liver microsomes: comparison of two proteomic methods and correlation with catalytic activity. *Drug Metab Dispos* **45**:1102-1112.

Adams JL, Greener BN, Kashuba ADM (2013) Pharmacology of HIV Integrase Inhibitors. *Curr Opin HIV AIDS* **7**: 390-400.

Argikar UA, Potter PM, Hutzler JM, Marathe PH (2016) Challenges and opportunities with non-CYP enzymes aldehyde oxidase, carboxylesterase, and UDP-glucuronosyltransferase: focus on reaction phenotyping and prediction of human clearance. *AAPS J* **18:** 1391-1405.

Al-Jahdari WS, Yamamoto K, Hiraoka H, Nakamura K, Goto F, Horiuchi R (2006) Prediction of total propofol clearance based on enzyme activities in microsomes from human kidney and liver. *Eur J Clin Pharmacol* **62**:527-33.

Belkhir L, Seguin-Devauz C, Laure E, Pauly C, Gengler N, Schneider S, Ruelle J, Haufroid V, Vandercam B. (2018) Impact of UGT1A1 polymorphisms on raltegravir and its glucuronide plasma concentrations in a cohort of HIV-1 infected patients. *Scientific Reports* **8**: 7359.

Boase S and Miners JO (2002) *In vitro-in vivo* correlations for drugs eliminated by glucuronidation: investigations with the model substrate zidovudine. *BR J Clin Pharmacol* **54**: 493-503.

Bowers GD, Culp A, Reese MJ, Tabolt G, Moss L, Piscitelli S, Huynh P, Wagner D, Ford SL, Gould EP, Pan R, Lou Y, Margolis DA, Spreen WR (2016) Disposition and

metabolism of cabotegravir: a comparison of biotransformation and excretion between different species and routes of administration in humans. *Xenobiotica* **46**:147-62.

Castellino S, Moss L, Wagner D, Borland J, Song I, Chen S, Lou Y, Min SS, Goljer I, Culp A, Piscitelli SC, Savina PM (2013) Metabolism, excretion, and mass balance of the HIV-1 integrase inhibitor dolutegravir in humans. *Antimicrob Agents Chemother* **57**: 3536-46.

Center for Disease Control and Prevention (2018) HIV in the United States Statistics Overview. Retrieved from: https://www.cdc.gov/hiv/statistics/overview/index.html

Chen S, Jean PS, Borland J, Song I, Yeo AJ, Piscitelli S, Rubio JP (2014) Evaluation of the effect of UGT1A1 polymorphisms on dolutegravir pharmacokinetics. *Pharmacogenomics* **15**: 9-16.

Court MH, Zhang X, Ding X, Yee KK, Hesse LM, Finel M (2012) Quantitative distribution of mRNAs encoding the 19 human UDP-glucuronosyltransferase enzymes in 26 adult and 3 fetal tissues*. Xenobiotica* **42**: 266-77.

Davies B and Morris T (1993) Physiological Parameters in Laboratory Animals and Humans. *Pharm Res* **10**: 1093-1095.

Drodzik M, Busch D, Lapczuk J, Muller J, Ostrowski M, Kurzawski M, Oswald S (2017) protein abundance of clinically relevant drug-metabolizing enzymes in the human liver and intestine: a comparative analysis in paired tissue specimens. *Clin Pharmacol Ther*. [Epub ahead of print]

Flexner C. Modern Human Immunodeficiency Virus Therapy: Progress and Prospects (2019) *Clin Pharmacol Ther* **105**:61-70.

Food and Drug Administration, Office of Clinical Pharmacology Review (2015) 204790 Dolutegravir (Tivicay®).

Gilead Sciences, Inc. (2017) Biktarvy: Multi-Discipline Review/Summary, Clinical, Non-Clinical. Retrieved from: https://www.accessdata.fda.gov/drugsatfda_docs/nda/2018/210251Orig1s000TOC.cfm

Gill KL, Houston JB, Galetin A (2012) Characterization of *in vitro* glucuronidation clearance of a range of drugs in human kidney microsomes: comparison with liver and intestinal glucuronidation and impact of albumin. *Drug Metab Dispos* **40**:825-35.

Gill KL, Gertz M, Houston JB, Galetin A (2013) Application of a physiologically based pharmacokinetic model to assess propofol hepatic and renal glucuronidation in isolation: utility of *in vitro* and *in vivo* data. *Drug Metab Dispos* **41**: 744-753.

Guidelines for the use of antiretroviral agents in adults and adolescents living with HIV (Updated:2018) U.S. Department of Health and Human Services.

Guillemette C, Levesque E, Rouleau M (2014) Pharmacogenomics of human uridine diphospho-glucuronosyltransferases and clinical implications. *Clin Pharmacol Ther* **96**: 324-339.

Gufford BT, Barr JT, Gonzalez-Perez V, Layton ME, White JR, Oberlies NH, Paine MF (2015) Quantitative prediction and clinical evaluation of an unexplored herb-drug interaction mechanism in healthy volunteers. *CPT Pharmacometrics Syst Pharmacol* **4**: 701-710.

Houston JB and Kenworthy KE (2000) *In vitro-in vivo* scaling of CYP kinetic data not consistent with the classical Michaelis−Menten Model. *Drug Metab Dispos* **28**: 246-254.

Izukawa T, Nakajima M, Fujiwara R, Yamanaka H, Fukami T, Takamiya M, Aoki Y, Ikushiro S, Sakaki T, Yokoi T (2009) Quantitative analysis of UDP-glucuronosyltransferase (UGT) 1A and UGT2B expression levels in human livers. *Drug Metab Dispos* **37**: 1759-1768.

Kassahun K, McIntosh I, Cui D, Hreniuk D, Merschman S, Lasseter K, Azrolan N, Iwamoto M, Wagner JA, Wenning LA (2007) Metabolism and disposition in human of raltegravir (MK-0518) an anti-AIDS drug targeting the human immunodeficiency virus 1 integrase inhibitor. *Drug Metab Dispos* **35**: 1657-63.

Komora H and Iwaki M (2011) *In vitro* and *in vivo* small intestinal metabolism of CYP3A and UGT substrates in preclinical animal species and humans: species differences. *Drug Metabolism Reviews* **43**: 476-498.

Laufer R, Gonzalez Paz O, Di Marco A, Bonelli F, Monteagudo E, Summa V, Rowley M (2009) Quantitative prediction of human clearance guiding the development of raltegravir (MK-0518, Isentress) and related HIV integrase inhibitors. *Drug Metab Dispos* **37**: 873-883.

Lee LS, Seng K, Wang L, Yong W, Hee K, Soh TI, Wong A, Cheong PF, Soong R, Sapari NS, Soo R, Fan L, Lee S, Goh BC (2016) Phenotyping of UGT1A1 activity using raltegravir predicts pharmacokinetics and toxicity of irinotecan in FOLFIRI. *PLoS ONE* **11**: e0147681.

Malaty LI and Kuper KK (1999) Drug interactions of HIV protease inhibitors. *Drug Saf* **20**: 147-69.

Margaillan G, Rouleau M, Fallon JK, Caron P, Villeneuve L, Turcotte V, Smith PC, Joy MS, Guillemette C (2015) Quantitative profiling of human renal UDP-glucuronosyltransferase and glucuronidation activity: a comparison of normal and tumoral kidney tissue. *Drug Metab Dispos* **43**: 611-619.

Mathias AA, West S, Hui J, Kearney BP. Dose-response of ritonavir on hepatic CYP3A activity and elvitegravir oral exposure (2009) *Clin Pharmacol Ther* **85**:64-70.

Ohno S, Kawana K, Nakajin S (2008) Contribution of UDP-Glucuronosyltransferase 1A1 and 1A8 to morphine-6-glucuronidation and its kinetic properties. *Drug Metab Dispos* **34**: 688-94.

Paine MF, Khalighi M, Fisher JM, Shen DD, Kunze KL, Marsh CL, Perkins JD, Thummel KE (1997) Characterization of interintestinal and intraintestinal variations in human CYP3A-dependent metabolism. *J Pharmacol Exp Ther* **283**:1552-62.

Pau A and George J (2015) Antiretroviral Therapy: Current Drugs*. Infect Dis Clin North Am* **28**: 371-402.

Quinn TC (2008) HIV epidemiology and the effects of antiviral therapy on long-term consequences*. AIDS* **22**: 7-12.

Reese MJ, Savina PM, Generaux GT, Tracey H, Humphreys JE, Kanaoka E, Webster LO, Harmon KA, Clarke JD, Polli JW (2013) *In vitro* investigations into the roles of drug transporters and metabolizing enzymes in the disposition and drug interactions of dolutegravir, a HIV integrase inhibitor. *Drug Metab Dispos* **41**: 353-61.

Soars MG, Burchelll B, Riley RJ (2002) *In vitro* analysis of human drug glucuronidation and prediction of *in vivo* metabolic clearance. *J Pharmacol Exp Ther* **301**: 382-90.

Song I, Borland J, Arya N, Wynne B, Piscitielli S (2015) Pharmacokinetics of dolutegravir when administered with mineral supplements in healthy adult subjects. *J Clin Pharmacol* **55**: 490-496.

Strassburg CP, Kneip S, Topp J, Obermayer-Straub P, Barut A, Tukey RH, Manns MP (2000) Polymorphic gene regulation and interindividual variation of UDP-glucuronosyltransferase activity in human small intestine. *J Biol Chem* **275**: 36164-36171.

Sun L, Wu J, Du F, Chen X, Chen ZJ (2013) Cyclic GMP-AMP synthase is a cytosolic DNA sensor that activates the type I interferon pathway. *Science* **339**:786-91.

Trezza C, Ford SL, Spreen W, Pan R, Piscitelli S (2015) Formulation and pharmacology of long-acting cabotegravir. *Curr Opin HIV AIDS* **10**: 239-45.

ViiV Healthcare (2013) Tivicay: Clinical Pharmacology Biopharmaceutics Review(s). Retrieved from: https://www.accessdata.fda.gov/drugsatfda_docs/nda/2013/204790Orig1s000TOC.cfm

Wenning LA, Petry AS, Kost JT, Jin B, Breidinger SA, DeLepeleire I, Carlini EJ, Young S, Rushmore T, Wagner F, Lunde NM, Bieberdorf F, Greenberg H, Stone JA, Wagner JA, Iwamoto M (2009) Pharmacokinetics of raltegravir in individuals with UGT1A1 polymorphisms. *Clin Pharmacol Ther* **85**: 623-627.

Williams JA, Hyland R, Jones BC, Smith DA, Hurst S, Goosen TC, Peterkin V, Koup JR, Ball SE (2004) Drug-drug interactions for UDP-glucuronosyltransferase substrates: a pharmacokinetic explanation for typically observed low exposure (AUCi/AUC) ratios. *Drug Metab Dispos* **32**: 1201-8.

Wood FL, Houston JB, Hallifax D (2017) Clearance Prediction Methodology Needs Fundamental Improvement: Trends Common to Rat and Human Hepatocytes/Microsomes and Implications for Experimental Methodology. *Drug Metab Dispos* **45**:1178-1188.

World Health Organization (2019) HIV/AIDS Global Health Observatory (GHO) Data. Retrieved from: https://www.who.int/gho/hiv/en/

Yagura H, Watanabe D, Ashida M, Kushida H, Hirota K, Ikuma M, Ogawa Y, Yajima K, Kasai D, Nishida Y, Uehira T, Yoshino M, Shirasaka T (2015) Correlation between UGT1A1 polymorphisms and raltegravir plasma trough concentrations in Japanese HIV-1-infected patients. *J Infect Chemother* **21**:713-7.

Yagura H, Watanabe D, Kushida H, Tomishima K, Togami H, Hirano A, Takahashi M, Hirota K, Ikuma M, Kasai D, Nishida Y, Yoshino M, Yamazaki K, Uehira T, Shirasaka T (2017) Impact of UGT1A1 gene polymorphisms on plasma dolutegravir trough concentrations and neuropsychiatric adverse events in Japanese individuals infected with HIV-1. *BMC Infect Dis* **17:**622.

Footnotes

a. This work was supported in part by the Indiana Center for AIDs Research and grants from the National Institute of Health/National Institute of General Medical Sciences (NIH/NIGMS) [Grants R01s GM078501 and GM121707 (Z.D)]. S.N.L and B.T.G supported by the National Institute of General Medical Sciences [Grant T32 GM008425]. B.T.G. also supported by the Indiana Clinical and Translational Sciences Institute Young Investigator Award [Grant UL1 TR001108].

b. Reprint requests: Zeruesenay Desta, PhD

Department of Medicine, Division of Clinical Pharmacology

Indiana University School of Medicine

950 W. Walnut Street, R2, Room 425

Indianapolis, IN 46202-5188

Phone: (317) 274-2823

Fax: (317) 278-2765

Email: zdesta@iu.edu

Figure Legends

Figure 1. Chemical structures of cabotegravir, dolutegravir and raltegravir and their respective O-glucuronides (cabotegravir glucuronide, dolutegravir glucuronide and raltegravir glucuronide). Red is the site of O-glucuronidation.

Figure 2. (A) Cabotegravir, **(B)** dolutegravir and **(C)** raltegravir glucuronidation kinetics in HLMs, HIMs, and HKMs. The substrate concentration versus velocity data were fit to Michaelis−Menten equation. Dots represent observed data and solid lines are predicted.

Figure 3. Reaction phenotyping with rUGT panel (0.2 mg/mL protein) for 50μM **(A)** cabotegravir **(B)** dolutegravir and **(C)** raltegravir. INSTIs glucuronide formation using a panel of rUGT isoforms.

Figure 4. (1) Cabotegravir, **(2)** dolutegravir and **(3)** raltegravir glucuronidation kinetics in **(A)** UGT1A1- and **(B)** UGT1A9-overexpressing baculovirus-insect cell system. The substrate concentration versus velocity data were fit to appropriate enzyme kinetic equation (see Table 2). Dots represent observed data and solid lines are predicted.

Figure 5. 1) Cabotegravir, **(2)** dolutegravir and **(3)** raltegravir glucuronidation kinetics in **(A)** UGT1A1- and **(B)** UGT1A9-overexpressing human embryonic kidney cell lysates. The substrate concentration versus velocity data were fit to appropriate enzyme kinetic equation (see Table 3). Dots represent observed data and solid lines are predicted.

Figure 6. Application of PBPK model to predict pharmacokinetics of a single 50 mg oral dose dolutegravir from *in vitro* data. Predicted mean concentration versus time profiles (solid lines), with 95th and 5th percentiles (dashed lines), incorporating *in vitro* glucuronidation kinetics in a step-wise approach from **(A)** HLMs, **(B)** HLMs and HIMs, and **(C)** HLMs, HIMs, HKMs overlaid with observed clinical data (dots) are shown.

DMD Fast Forward. Published on February 25, 2019 as DOI: 10.1124/dmd.118.085035
This article has not been copyedited and formatted. The final version may differ from this version.

Table 1. Glucuronidation kinetic parameters from pooled human microsomal preparations.

Enzyme source	$f_{u,inc}$	$K_{m,u}$ (µM)	V_{max} (pmol/min/ mg protein)	$Cl_{int,u}$ (µl/min/mg mics)	$Cl_{int,organ}$ (L/h/ organ)
			Cabotegravir		
HLMs	0.52	350 (41)	705 (35)	2.0	8.1
HIMs	0.69	*	1031 (323)	ND*	ND*
HKMs	0.50	560 (57)	1088 (56)	1.9	0.45
			Dolutegravir		
HLMs	0.23	32 (2)	601(13)	18	76
HIMs	0.37	96 (7)	1170 (33)	12	2.1
HKMs	0.29	47 (8)	291 (16)	6.2	1.1
			Raltegravir		
HLMs	1	183 (23)	1737 (63)	9.5	38.7
HIMs	1	167 (23)	326 (13)	2.0	0.3
HKMs	0.97	493 (59)	2332 (111)	4.7	0.5

Values represent the parameter estimate (SE) by fitting the simple MichaelisMenten equation ($v=V_{max} *[S]/K_m+[S]$) to metabolite formation velocity using Phoenix WinNonlin (v. 7.0). Cl_{int} calculated as the ratio of V_{max} to K_m.

*The substrate concentration versus velocity did not saturate and the estimated K_m (> 6mM) and V_{max} values were unreliable. Thus, the values are not presented and $Cl_{int,u}$ and $Cl_{int,organ}$ were not determined (ND).

DMD Fast Forward. Published on February 25, 2019 as DOI: 10.1124/dmd.118.085035
This article has not been copyedited and formatted. The final version may differ from this version.

Table 2. Glucuronidation kinetic parameters from UGT-overexpressing in baculosomal cell system.

Enzyme source	Model	$K_{m,u}$ or $S_{50,u}$ (µM)	V_{max} (pmol/min/mg of total protein)	n	$Cl_{int,u}$ or $Cl_{max,u}$ (µl/min/mg protein)
		Cabotegravir			
rUGT1A1	Two Site	27 (6)*	17 (1)*		0.6
rUGT1A3	MM	46 (7)	3 (0.1)		0.06
rUGT1A7	MM	43 (5)	10 (0.3)		0.2
rUGT1A8	MM	344 (44)	40 (2)		0.1
rUGT1A9	Hill	56 (7)	61.4 (3)	1.26 (0)	1.1
		Dolutegravir			
rUGT1A1	MM	216 (26)	507 (50)		2.3
rUGT1A3	MM	62 (7)	18 (0.7)		0.3
rUGT1A7	MM	9 (2)	1 (0)		0.1
rUGT1A8	Hill	44 (5)	7 (0)	1.9 (0)	0.2
rUGT1A9	Hill	39 (3)	39 (2)	1.9 (0)	1.0
		Raltegravir			
rUGT1A1	MM	260 (17)	334 (7)		1.3
rUGT1A3	Hill	41 (2)	30 (1)	1.7 (0)	0.55
rUGT1A7	MM	452 (56)	23 (1)		0.05
rUGT1A8	MM	386 (57)	39 (2)		0.1
rUGT1A9	Hill	193 (12)	459 (14)	1.45 (0)	1.3

*The low affinity enzyme substrate concentration versus velocity did not saturate and the estimated K_m (> 2mM) and V_{max} values were unreliable. Thus, only the high K_m is presented and calculated for $Cl_{int,u}$.

- *n* is the hill coefficient in the Hill equation.

Values represent the parameter estimate (SE) by fitting the simple Michaelis-Menten (MM), Hill, or Two Site equation as described in the methods to metabolite formation velocity using Phoenix WinNonlin (v. 7.0). $Cl_{int} = V_{max}/K_m$ or $Cl_{max} = (\frac{Vmax}{km} \times \frac{(n-1)}{n(n-1)^{\frac{1}{n}}})$.

DMD Fast Forward. Published on February 25, 2019 as DOI: 10.1124/dmd.118.085035
This article has not been copyedited and formatted. The final version may differ from this version.

Table 3. Glucuronidation kinetic parameters from UGT-overexpressing in HEK cell system.

Enzyme source	Model	$K_{m,u}$ or $S_{50,u}$ (µM)	V_{max} (pmol/min/mg of total protein)	n	$Cl_{int,u}$ or $Cl_{max,u}$ (µl/min/mg protein)
		Cabotegravir			
HEKUGT1A1	MM	55 (9)	7 (0)		0.1
HEKUGT1A7	MM	23 (6)	9 (0)		0.3
HEKUGT1A8	MM	133 (5)	12 (0)		0.09
HEKUGT1A9	MM	163 (6)	25 (0)		0.2
		Dolutegravir			
HEKUGT1A1	MM	96 (15)	21 (1)		0.2
HEKUGT1A7	Hill	2 (3)	2 (0)	1.4 (0)	1.1
HEKUGT1A8	Hill	37 (2)	36 (1)	1.4 (0)	1.0
HEKUGT1A9	Hill	46 (3)	107 (4)	1.7 (0)	2.3
		Raltegravir			
HEKUGT1A1	Hill	52 (7)	17 (1)	1.5 (0)	0.4
HEKUGT1A3	Hill	22 (1)	2 (0)	1.7 (0)	0.05
HEKUGT1A7	MM	79 (8)	6 (0)		0.07
HEKUGT1A8	Hill	142 (15)	6 (0)	1.4 (0)	0.1
HEKUGT1A9	Hill	219 (29)	24 (1.4)	1.5 (0)	0.06

- *n* is the hill coefficient in the Hill equation.

Values represent the parameter estimate (SE) by fitting the simple Michaelis-Menten (MM) or Hill equation as described in the methods to metabolite formation velocity using Phoenix WinNonlin (v. 7.0). $Cl_{int} = V_{max}/K_m$ or $Cl_{max} = (\frac{Vmax}{km} \times \frac{(n-1)}{n(n-1)^{\frac{1}{n}}})$.

Table 4. Dolutegravir clinical pharmacokinetic outcomes recovered from observed data and PBPK model predictions (geometric mean, CV% incorporating *in vitro* glucuronidation kinetics data from (1) HLMs only, (2) HLMs and HIMs, and (3) HLMs, HIMs, HKMs.

	C_{max} (µg/mL)	$AUC_{0-\infty}$ (µg·h/mL)	Cl_{PO} (L/h)	$t_{1/2}$ (h)	fm (%) Liver	fm (%) Kidney	fg (%)	fh (%)	fa (%)
Observed	2.2 (43)	43.7 (45)	1.1 (45)	14.4 (19)			N/A		
HLMs only	5.8 (19)	199.6 (55)	0.3 (50)	21.1 (40)	99.2	0.8	98	99	100
HLMs and HIMs	2.7 (24)	89.4 (55)	0.56 (50)	21.1 (40)	99.2	0.8	46	99	100
HLMs, HIMs, HKMs	2.6 (24)	60.4 (43)	0.8 (44)	15.3 (37)	79.7	20.3	46	99	100

DMD Fast Forward. Published on February 25, 2019 as DOI: 10.1124/dmd.118.085035
This article has not been copyedited and formatted. The final version may differ from this version.

Table 5. Summary of the tissue- and isoform- specific UGTs responsible for cabotegravir, dolutegravir, and raltegravir metabolism based on relations of K_m values derived from expression systems.

	HLMs	HIMs	HKMs
Cabotegravir	UGT1A1*	ND	ND
Dolutegravir	UGT1A9 > UGT1A1*	UGT1A3 > UGT1A8 > UGT1A1*	UGT1A9
Raltegravir	UGT1A9 > UGT1A1	UGT1A8 > UGT1A1	UGT1A9

* Isoform UGT K_m value greater than 2-fold difference from that observed for the tissue K_m value

ND = not determine

DMD Fast Forward. Published on February 25, 2019 as DOI: 10.1124/dmd.118.085035
This article has not been copyedited and formatted. The final version may differ from this version.

Figure 1

Cabotegravir

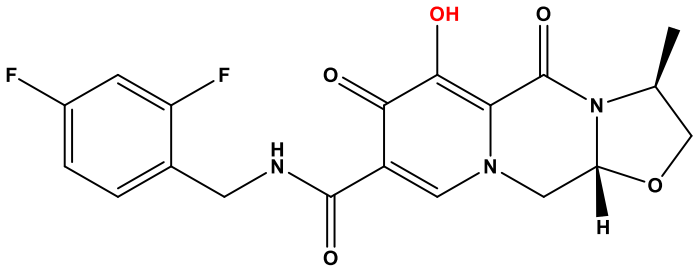

Cabotegravir glucuronide

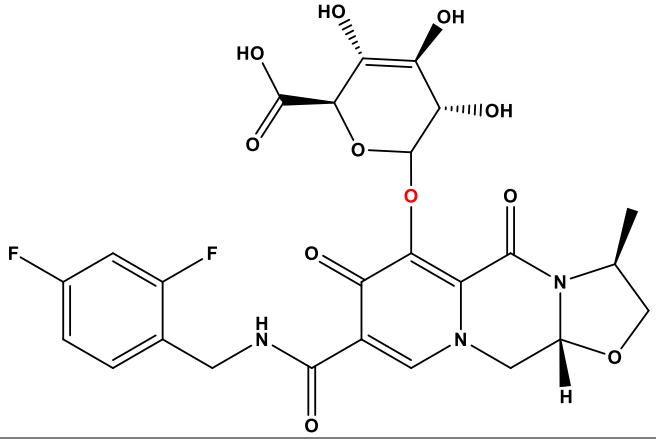

Dolutegravir

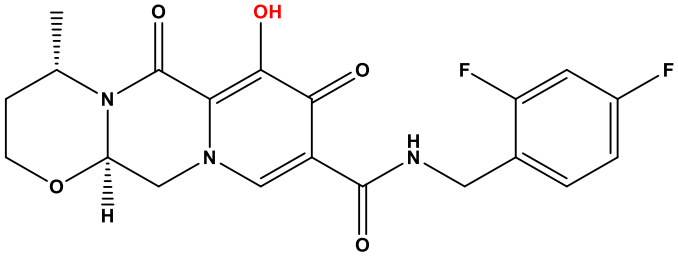

Dolutegravir glucuronide

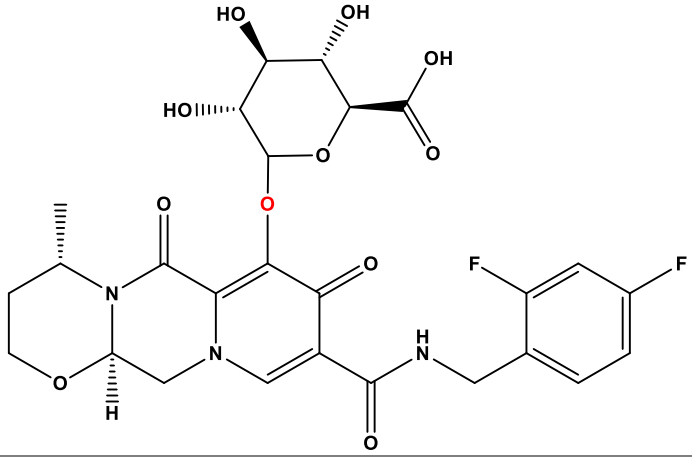

Raltegravir

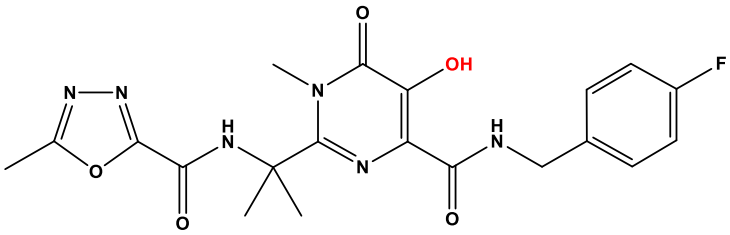

Raltegravir glucuronide

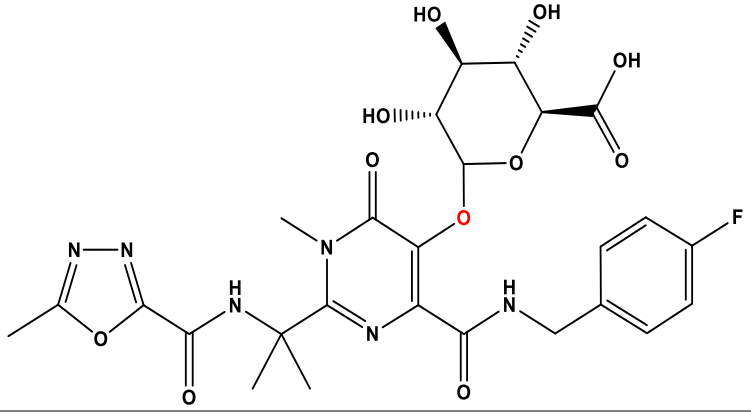

DMD Fast Forward. Published on February 25, 2019 as DOI: 10.1124/dmd.118.085035
This article has not been copyedited and formatted. The final version may differ from this version.

Figure 2

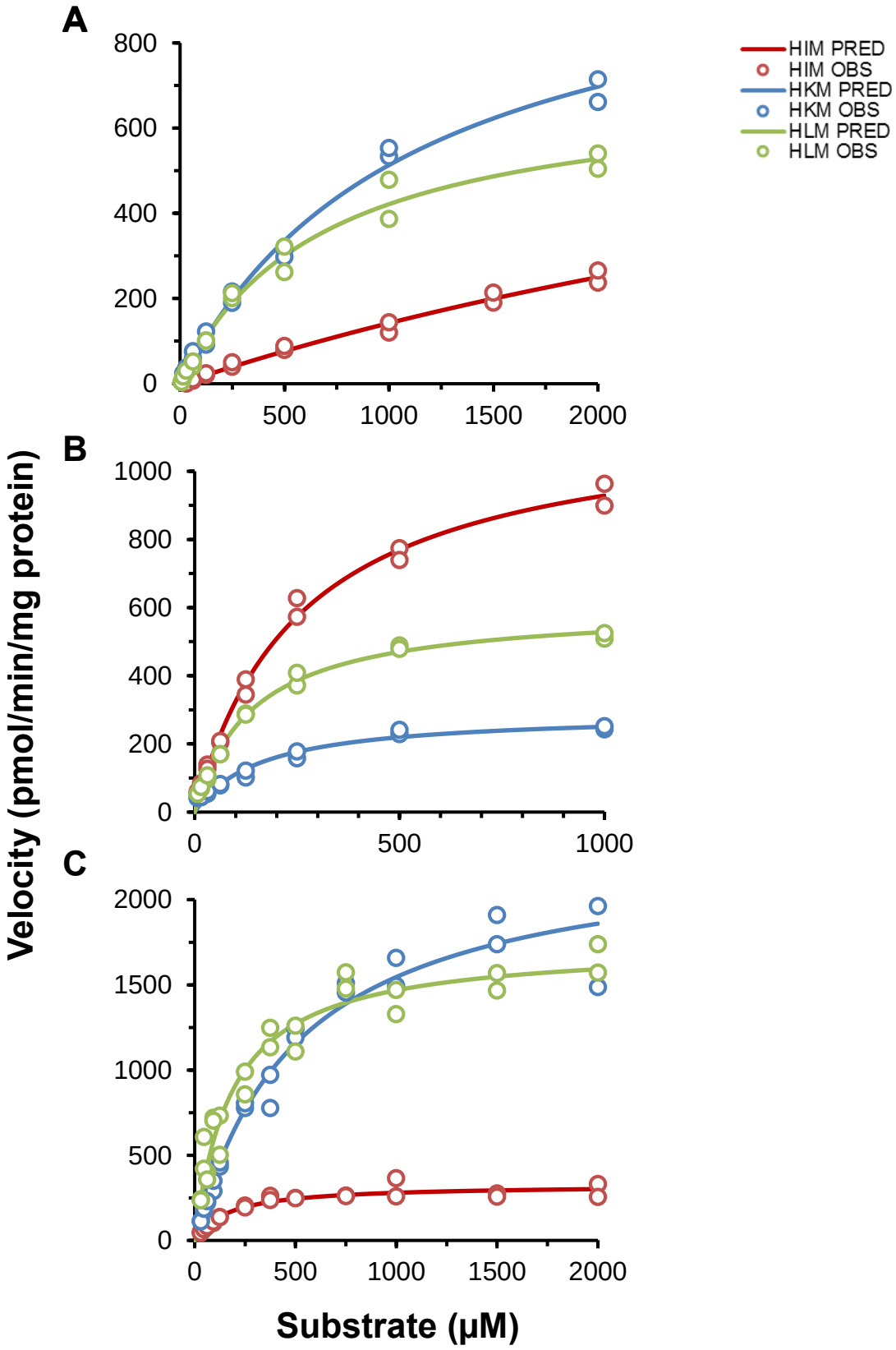

DMD Fast Forward. Published on February 25, 2019 as DOI: 10.1124/dmd.118.085035
This article has not been copyedited and formatted. The final version may differ from this version.

Figure 3

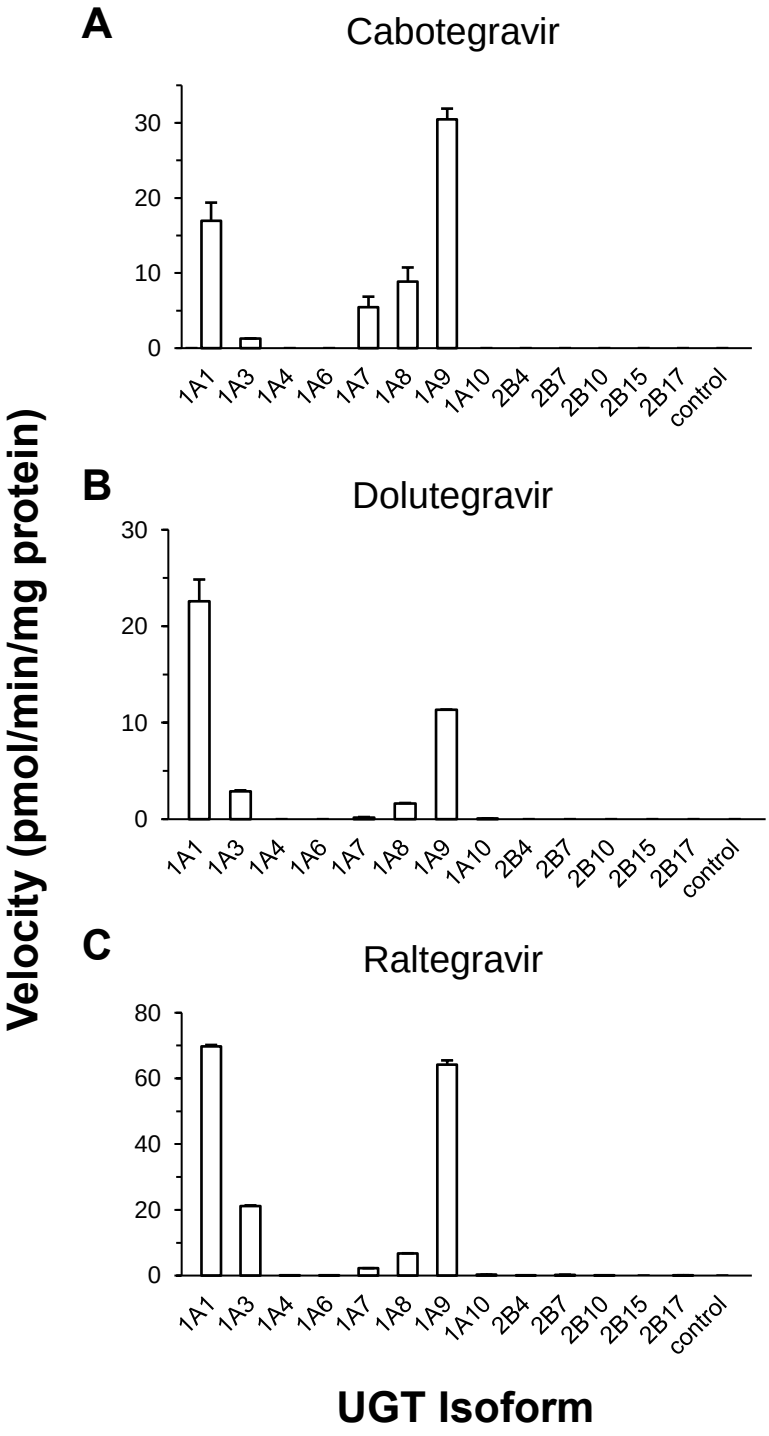

DMD Fast Forward. Published on February 25, 2019 as DOI: 10.1124/dmd.118.085035
This article has not been copyedited and formatted. The final version may differ from this version.

Figure 4

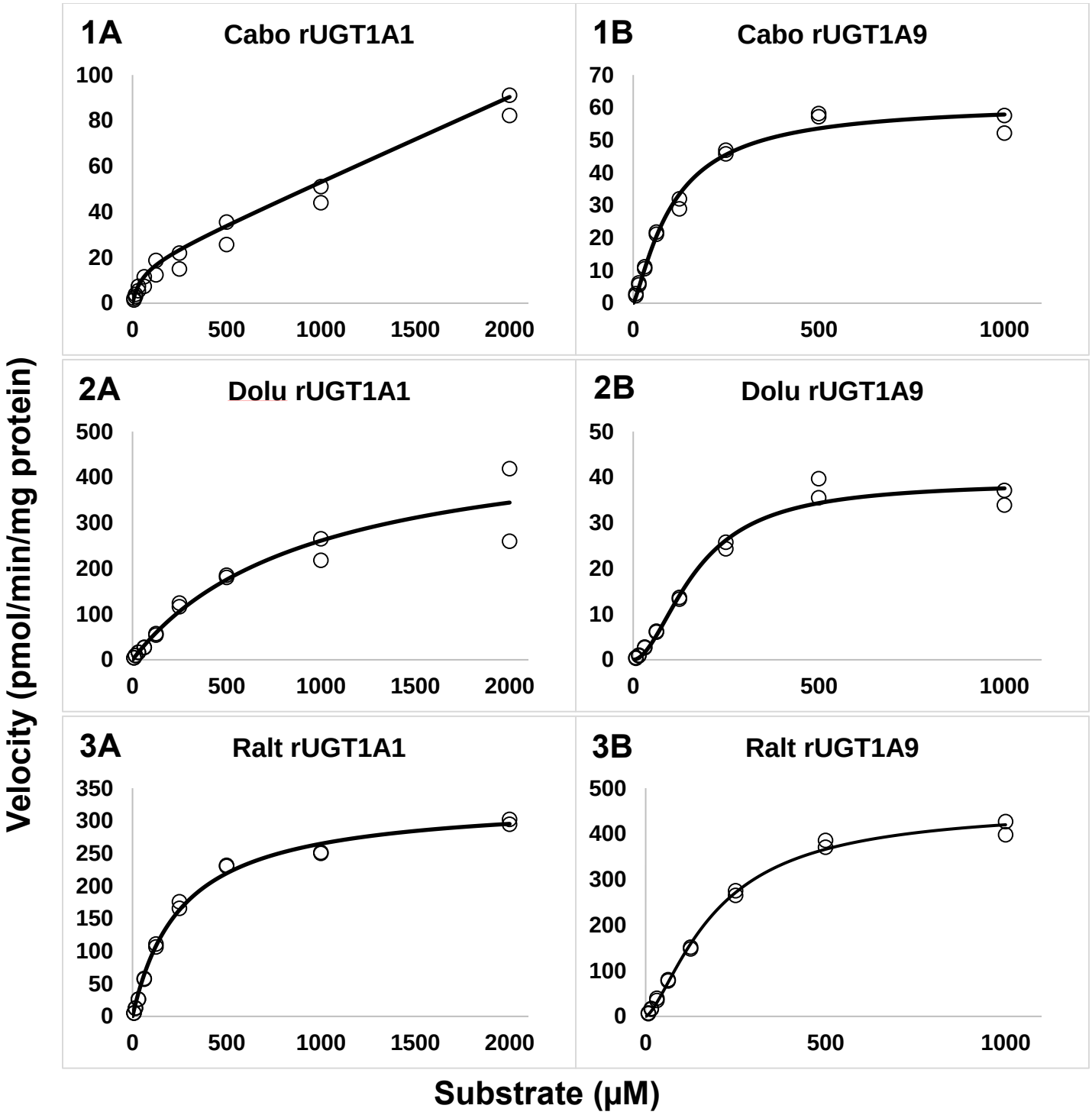

DMD Fast Forward. Published on February 25, 2019 as DOI: 10.1124/dmd.118.085035
This article has not been copyedited and formatted. The final version may differ from this version.

Figure 5

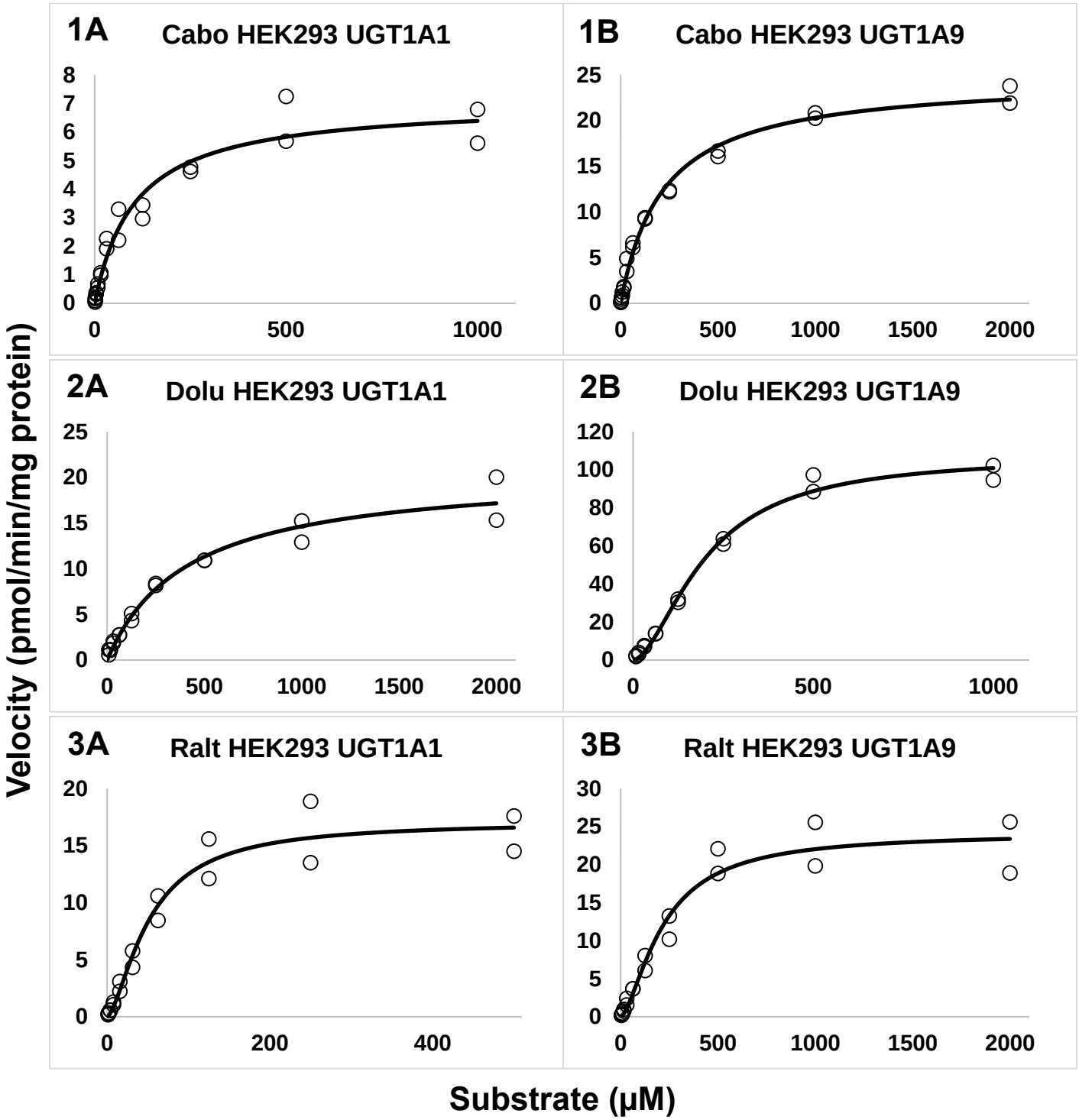

DMD Fast Forward. Published on February 25, 2019 as DOI: 10.1124/dmd.118.085035
This article has not been copyedited and formatted. The final version may differ from this version.

Figure 6

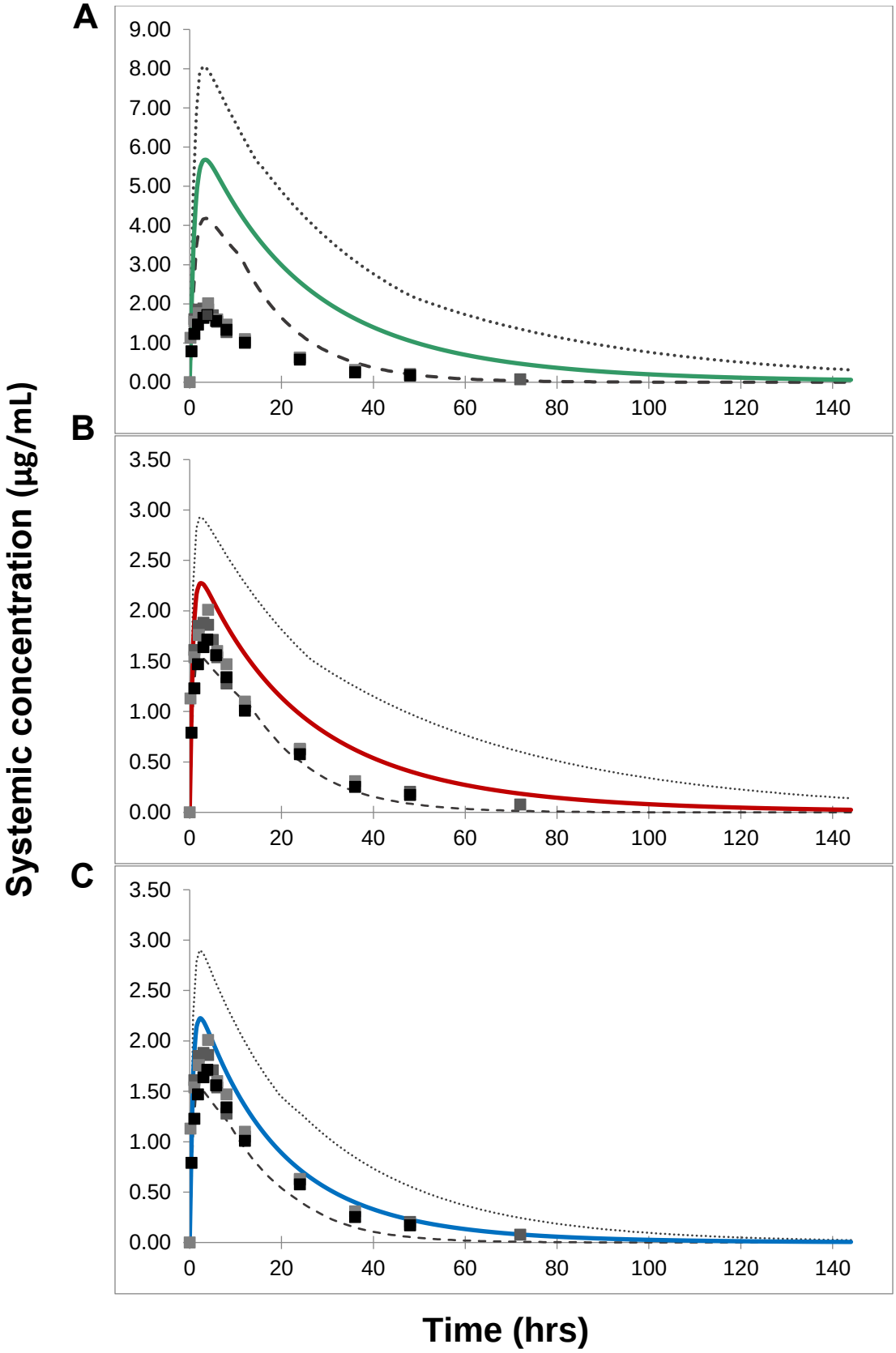

Mechanistic Assessment of Extrahepatic Contributions to Glucuronidation of Integrase Strand Transfer Inhibitors

Stephanie N. Liu[1], Jessica Bo Li Lu[1], Christy J.W. Watson[2], Philip Lazarus[2], Zeruesenay Desta[1], and Brandon T. Gufford[1]

[1]Division of Clinical Pharmacology, Department of Medicine, School of Medicine, Indiana University, Indianapolis, IN

[2]Department of Pharmaceutical Sciences, College of Pharmacy and Pharmaceutical Sciences, Washington State University, Spokane, WA

Supplemental Materials

(Additional Supplemental File attached includes details of the SimCyp substrate file and simulated trial design)

Supplemental Figure 1. HPLC-MS/MS chromatogram for cabotegravir, dolutegravir, raltegravir, and their respective glucuronide in (A) positive ionization mode and (B) negative ionization mode using authentic standards.

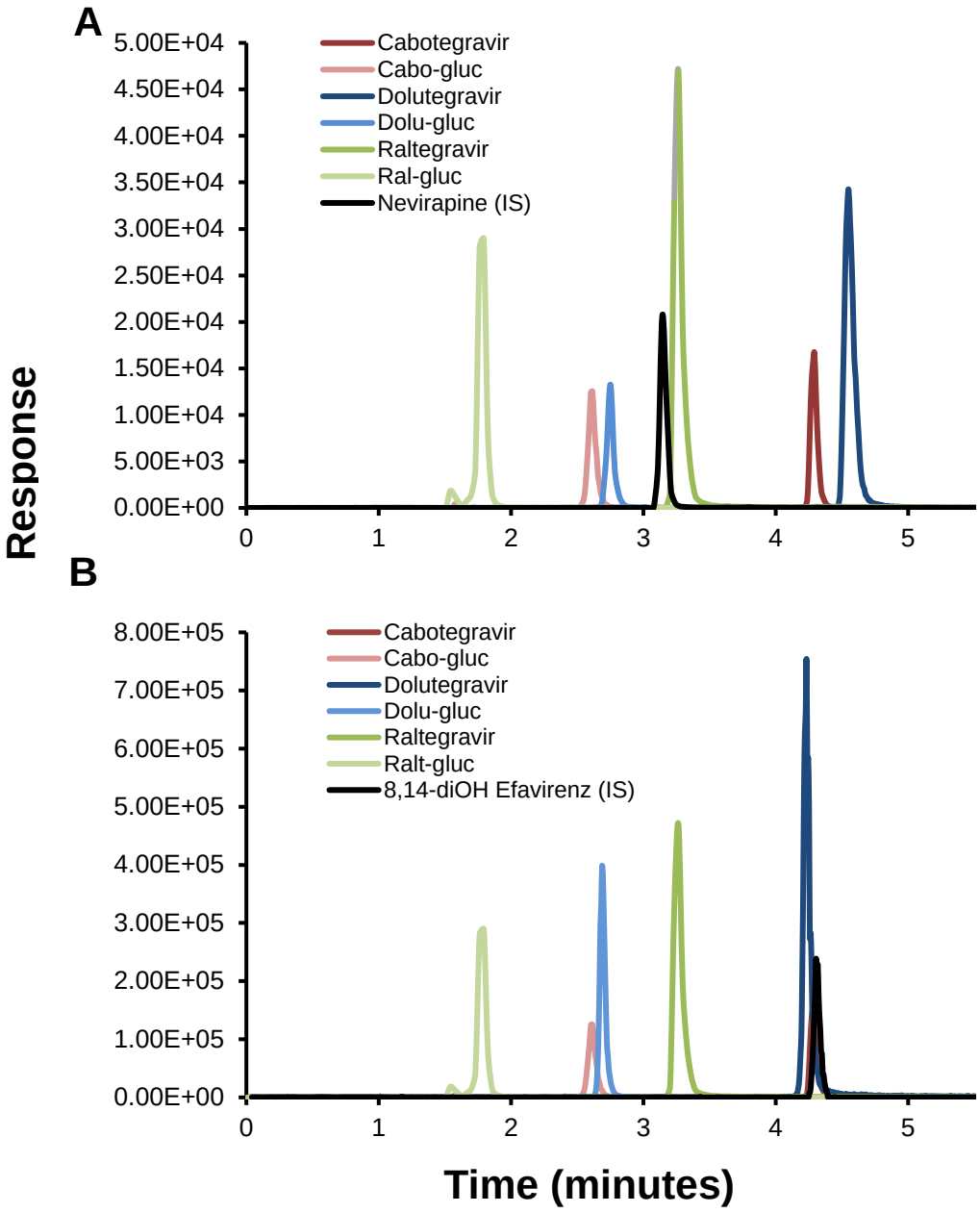

Supplemental Figure 2. *In vitro* extrahepatic glucuronidation clearance parameter sensitivity analysis on dolutegravir pharmacokinetic parameters.

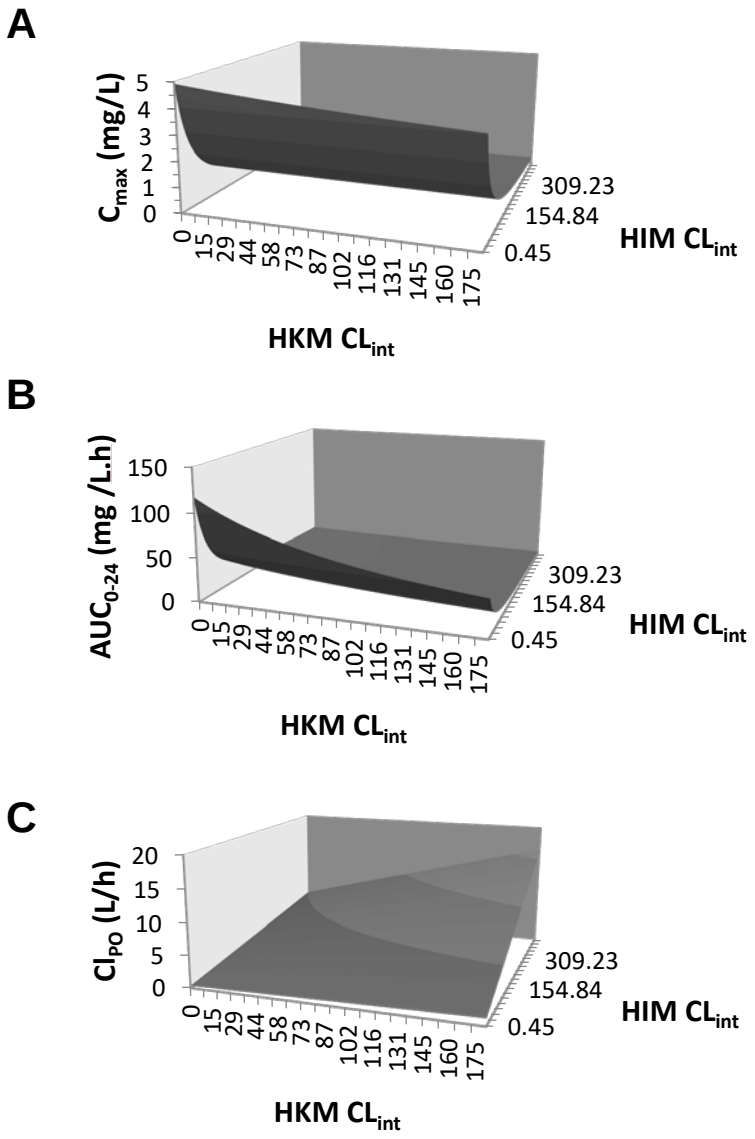

Supplemental Table 1. Analyte mass spectrometry parameters (negative and positive mode).

Analyte	Declustering potential (V)	Collision energy (mV)	*m/z* conversions
Cabotegravir glucuronide	-75	-46	580.1→374.1
Dolutegravir glucuronide	-96	-30	594.0→418.0
Raltegravir glucuronide	-70	-38	619.2→316.1
8,14-diOH EFV (-IS)	-45	-30	346.1→238.1

Analyte	Declustering potential (V)	Collision energy (mV)	*m/z* conversions
Cabotegravir	147	32	406.0→263.1
Cabotegravir glucuronide	40	50	445.1→109.1
Dolutegravir	160	39	420.1→277.1
Dolutegravir glucuronide	113	54	596.0→277.2
Raltegravir	70	33	445.1→109.1
Nevirapine (+IS)	135	34	266.9→226.1

Supplemental Table 2. Protein concentration, protein source, and incubation time for INSTI substrate.

Substrate	Protein Source	Protein Concentration (mg/mL)	Incubation Time (min)
Cabotegravir	Pooled HLM	0.5	60
	Pooled HKM	0.5	60
	Pooled HIM	0.5	60
	Reaction phenotyping rUGT panel	0.2	60
	rUGT1A1	0.1	60
	rUGT1A3	0.2	60
	rUGT1A7	0.1	120
	rUGT1A8	0.1	60
	rUGT1A9	0.1	60
	HEK293 UGT1A1	0.1	120
	HEK293 UGT1A7	0.1	120
	HEK293 UGT1A8	0.2	120
	HEK293 UGT1A9	0.2	60
	HEK293 UGT1A10	0.1	120
Dolutegravir	Pooled HLM	0.5	30
	Pooled HKM	0.5	30
	Pooled HIM	0.5	30
	Reaction phenotyping rUGT panel	0.2	60

	rUGT1A1	0.1	30
	rUGT1A3	0.1	30
	rUGT1A7	0.1	60
	rUGT1A8	0.1	30
	rUGT1A9	0.1	20
	HEK293 UGT1A1	0.1	30
	HEK293 UGT1A7	0.1	60
	HEK293 UGT1A8	0.05	30
	HEK293 UGT1A9	0.05	30
	HEK293 UGT1A10	0.1	60
Raltegravir	Pooled HLM	0.1	20
	Pooled HKM	0.1	20
	Pooled HIM	0.1	20
	Reaction phenotyping rUGT panel	0.2	60
	rUGT1A1	0.1	30
	rUGT1A3	0.05	30
	rUGT1A7	0.1	30
	rUGT1A8	0.1	30
	rUGT1A9	0.05	20
	HEK293 UGT1A1	0.1	30
	HEK293 UGT1A3	0.1	60
	HEK293 UGT1A7	0.1	30

	HEK293 UGT1A8	0.1	60
	HEK293 UGT1A9	0.1	30
	HEK293 UGT1A10	0.1	30

Supplemental Table 3. Dolutegravir PBPK Model Input Parameters.

Parameter	Value	Reference
Physiochemical properties		
Molecular Weight (g/mol)	419	FDA Tivicay 2015
Log $P_{o:w}$	2.16	FDA Tivicay 2015
Species	Monoprotic acid	Predicted via SimCyp
Protein Binding		
B/P	0.550	Castellino et al 2013
f_u	0.005	Castellino et al 2013
Absorption		
Simulation	ADAM	
MDCK II (10^{-6} cm/s)	265	Reese et al 2013
$P_{eff,man}$ (10^{-4} cm/s)	34.642	Predicted via SimCyp
In vivo pharmacokinetic properties (full PBPK model)		
V_{ss} (L/kg)	0.107	
Prediction Model	Method 3	
Metabolism: rCYP450 enzyme kinetics (Cl_{int}; µL/min/mg protein)		
CYP3A4	3.00	Reese et al 2013
Percentage available for enterohepatic recirculation	100%	SimCyp
Intestinal Transport (Cl_{int},T; µL/min)		
Apical Efflux (P-gp)	28	Castellino et al 2013
Apical Efflux (BCRP)	7.8	Castellino et al 2013

Simcyp Population Based Simulator

1/31/2019 14:31

Simcyp Version 16 (02/12/2016)

Substrate	
Compound Name	Wsp-Dolutegravir
Version number	Not applicable
Molecule Type	Small Molecule
Route	Oral
Dose Units	Dose (mg)
Dose	50.000
Start Day	1.000
Start Time	9h0m
Dosing Regimen	Single Dose
PhysChem and Blood Binding	
Mol Weight (g/mol)	419.000
log P	2.160
Compound Type	Monoprotic Acid
pKa 1	8.300
BP input type	User
B/P	0.550
Haematocrit	45.000
fu input	User
fu	0.005
Reference Binding Component	HSA
Protein Reference Conc (g/L)	45.000
% Bound to Lipoprotein	0.000
% Bound to Lipoprotein (CV %)	0.000
Absorption	
Absorption Model	ADAM
input type	Predicted
fa	1.000
ka (1/h)	15.126
fu(Gut) input type	User
fu(Gut)	1.000
Peff,man Type	Global
Peff,man (10-4 cm/s)	34.642
Permeability Assay	MDCK
MDCK(10E-06 cm/s)	265.000
Reference Compound	Cimetidine
Reference Compound Value (10E-06 cm/s)	6.600
Scalar	1.000
Degradation Rate Stomach (1/h)	0.000
Degradation Rate Duodenum (1/h)	0.000
Degradation Rate Jejunum I (1/h)	0.000
Degradation Rate Jejunum II (1/h)	0.000
Degradation Rate Ileum I (1/h)	0.000
Degradation Rate Ileum II (1/h)	0.000
Degradation Rate Ileum III (1/h)	0.000
Degradation Rate Ileum IV (1/h)	0.000
Degradation Rate Colon (1/h)	0.000
Input Form	Solid Formulation
Formulation	Immediate Release (IR)
Define Disintegration Profile	Not activated
Dissolution Type	Solubility
Solubility pH Type	Intrinsic
Solubility (mg/mL)	0.238
pH Surface Calculation	Off
Precipitation Model	Model 1
PRC (Precipitation Rate Constant)	Global
PRC (1/h)	4.000
CSR (Critical Supersaturation Ratio)	Global
CSR value	10.000
Reference Concentration for Precipitation Model	Total
Solubility Factor 1	10000.000
Dispersion Type	Monodispersed
Radius (µm)	10.000
DLM Scalar	All Segments
DLM Scalar values	1.000
Particle density (g/mL)	1.200
Viscosity Model	Off
Viscosity Model Exponent	0.987
Diffusion coeff. input type	Predicted
Diffusion coeff, ionised (10-4 cm2/min)	4.035
Diffusion coeff, micelle (10-4 cm2/min) mean	0.780
Diffusion coeff, micelle CV (%)	20.000

Trial Design	
Use Pop Representative	No
Population Size	100.000
Number of Trials	10.000
No of Subjects per Trial	10.000
Population name: Lib 1	Sim-Healthy Volunteers
Version number: Lib 1	16.0.0
No. of Subjects: Lib 1	100.000
Minimum Age: Lib 1 (years)	20.000
Maximum Age: Lib 1 (years)	50.000
Propn. of Females: Lib 1	0.500
Prandial State	Fasted
Fluid intake with dose (mL)	250.000
Fluid intake with dose CV (%)	30.000
PKPD Parameters	On
PKPD Profiles	On
Start Day/Time	Day 1, 09:00
End Day/Time	Day 7, 09:00
Study Duration (h)	144.000
Sub : Route	Oral
Random Generator	Mersenne Twister (MT19937)
Seed	Fixed
Seed Value	1.000
Solver sampling interval (h)	0.050
Sampling Time	Pre-defined Uniform
Number of time samples	200.000
Sampling Site Selection	Off
AUC Calculations (Substrate)	
Calculated AUCt first dose	Yes
Calculated AUC_INF	Yes
Calculated AUCt last dose	No
Integrated AUCt first dose	Yes
Integrated AUCt last dose	No
Integrated AUCt user interval	No
Method	Linear Up Log Down
Memory Size	4000000.000
Solubility Cap (mg/mL)	500.000
Differential Solver	5th-order Runge-Kutta
Maximum number of steps	1000000.000
Relative Tolerance	0.000
Relative Tolerance when ADAM is used	0.000
Integration error tolerance	0.001
Use UBL fluid volumes	Off
Apply Minimum Mass Limit(ADAM)	Off
Minimum Mass Limit	n/a
LUA Scripting(ADAM)	Off
Paediatric Module	Not Loaded
No. Differential Equations	110.000

Software Version Detail	
Simulation Duration(seconds)	95.000
Windows Version	Windows 10
Excel Version	Excel 2016
Source File Location	C:\Program Files\Simcyp\Simcyp Simulator V16\Screens\
Excel Embedded Workspace	Yes
Simcyp.exe	
File Version	16.0.113.0
Date Modified	02/12/2016
File Size (bytes)	2801664
Simcyp.UI.Common.dll	
File Version	15.0.0.0
Date Modified	02/12/2016
File Size (bytes)	1666048
Simcyp.ViewModel.Animal.dll	
File Version	15.0.0.0
Date Modified	02/12/2016
File Size (bytes)	71168
Simcyp.ViewModel.Common.dll	
File Version	16.0.113.0
Date Modified	02/12/2016
File Size (bytes)	468992
SimcypLicenceManager.dll	
File Version	1.0.0.2
Date Modified	02/12/2016
File Size (bytes)	86016
simcyp.ViewModel.dll	
File Version	16.0.113.0
Date Modified	02/12/2016
File Size (bytes)	526848
simcyp.licencing.dll	
File Version	16.0.113.0
Date Modified	02/12/2016
File Size (bytes)	57344
simcyp.model.XmlSerializers.dll	
File Version	15.0.6180.29192
Date Modified	02/12/2016
File Size (bytes)	3886592
simcyp.model.dll	
File Version	16.0.113.0
Date Modified	02/12/2016
File Size (bytes)	4397568
Login name	liuste
Computer name	IN-MDEP-160076
Licence type	Desktop
Key	AADDPFIAILALJIKCJL
Expiry	22-08-2019

Diffusion coeff. (10E-4 cm²/min)	4.035
heff method selected	Hintz-Johnson
heff cut-off type	Default
heff cut-off value (µm)	30.000
Bile Micelle mediated solubilisation	On
Bile solubilisation input type	Predicted
Bile Micelle Partition: Slope	0.740
Bile Micelle Partition: Offset	2.290
Bile Micelle Partition: Ionised Species Correction	1.000
Absorption Scalars (no units)	SI Global
Absorption Scalar SI Global	1.000
Absorption Scalar Colon	1.000
Segregated transit time model	Not activated
Distribution	
Distribution Model	Full PBPK Model
Replacement Organ?	No
Organ Replaced	n/a
User-defined Additional Organ	No
Type	n/a
Vss input type	Predicted
Vss (L/kg)	0.107
Prediction Method	Method 3
Subcellular Distribution	Off
Permeability Ratio: Monoanions	3.300
Permeability Ratio: Monocations	2.300
Permeability Ratio: Dianions	10.000
Permeability Ratio: Dications	10.000
Permeability Ratio: Ampholyte	2.000
Concentration-dependent volume	No
log Po:w	2.160
logP vo:w input type	Predicted
logP vo:w Prediction Method	Hansch
logP vo:w Hansch a	1.115
logP vo:w Hansch b	-1.350
logP vo:w	1.058
Compound Type	Monoprotic Acid
pKa 1	8.300
Adipose input type	Predicted
Adipose	0.077
Bone input type	Predicted
Bone	0.106
Brain input type	Predicted
Brain	0.089
Gut input type	Predicted
Gut	0.173
Heart input type	Predicted
Heart	0.171
Kidney input type	Predicted
Kidney	0.144
Liver input type	Predicted
Liver	0.107
Lung input type	Predicted
Lung	0.220
Muscle input type	Predicted
Muscle	0.043
Skin input type	Predicted
Skin	0.287
Spleen input type	Predicted
Spleen	0.113
Pancreas input type	Predicted
Pancreas	0.071
Kp Scalar	1.000
Smoothing Function	Off
Lipid Binding Scalar	1.000
Use Pvo:w for Neutral Lipid Partition in All Tissues	Yes
Elimination	
Allometric Scaling	Not Used
Clearance Type	Enzyme Kinetics
FI Correction	Not used
PLR Correction	Not Used
In vitro metabolic system	HLM
Pathway	Pathway 1
Enzyme	CYP3A4
CLint (µL/min/mg protein)	3.000
fu mic	1.000
In vitro metabolic system	HLM
Pathway 1	O-glucuronidation
Enzyme	UGT1A1
Vmax (pmol/min/mg protein)	602.000
Km (µM)	140.000
fu mic	0.230
Feed formed renal metabolite into kidney	No
Use Allelic variants for Enzyme 1	No
Enzyme	CYP2C9
Use Allelic variants for Enzyme 2	No
Enzyme	CYP1A2
Human intestine preparation method	HIMms

Additional HIM ms CLint (µL/min/mg protein)	45.000
Additional HIM ms CV (%)	30.000
Additional HIM ms fumic	0.370
Additional HKM CLint (µL/min/mg protein)	18.000
Additional HKM CV (%)	30.000
Additional HKM fumic	0.290
Ontogeny Profile	No Profile Used
Biliary CLint (Hep) (µL/min/10^6)	0.000
CV Biliary CLint (Hep) (%)	30.000
Ontogeny Profile	No Profile Used
Percentage available for re-absorption (%)	100.000
Active Uptake into Hepatocyte	1.000
CL R (L/h)	0.000
Organ/Tissue	Kidney
Transporter	SLC22A2 (OCT2)
Ki (µM)	1.900
fuinc (Ki)	1.000
Transporter	SLC22A6 (OAT1)
Ki (µM)	2.000
fuinc (Ki)	1.000
Transporter	SLC22A8 (OAT3)
Ki (µM)	2.000
fuinc (Ki)	1.000
Transporter	SLC47As (MATEs)
Ki (µM)	6.300
fuinc (Ki)	1.000
Transport	
Assume Colon SS	Yes
Organ/Tissue	Gut
Transporter	ABCB1 (P-gp/MDR1)
Location	Apical
Function	Efflux
CLint,T (µL/min)	28.000
A (cm^2)	1.000
System	MDCK
RAF/REF	1.500
Transporter	ABCG2 (BCRP)
Location	Apical
Function	Efflux
CLint,T (µL/min)	7.800
A (cm^2)	1.000
System	MDCK
RAF/REF	1.000